Material-by-Design as applied to Linear Antenna Array Performance Improvement

M. Salucci, G. Oliveri, N. Anselmi, G. Gottardi, and A. Massa

Abstract

This work deals with the problem of improving the radiation performances of linear active electronically scanned arrays (*AESA*s), without increasing the number of radiating elements nor requiring a re-design of the radiators and/or the feeding network. The problem is addressed by means of an innovative Material-by-Design (*MbD*) approach based on the quasi-conformal transformation optics (*QCTO*) technique and a customized source inversion (*SI*) strategy. The synthesized architectures are composed by a metamaterial lens and a tapered version of the original feeding network, able to match the radiation characteristics of significantly larger apertures. Some preliminary results are reported in order to validate the effectiveness of the proposed *MbD* approach.

1 Half-Cosine Profile - $h' = 4.0$ [λ], $l' = 1.0$ [λ], $t' = 10.0$ [λ], $N = 15$ - Analysis vs. w'

1.1 Step 1: Expanding the physical array ($N = 15$, $L = 7.0$ [λ])

Input Parameters

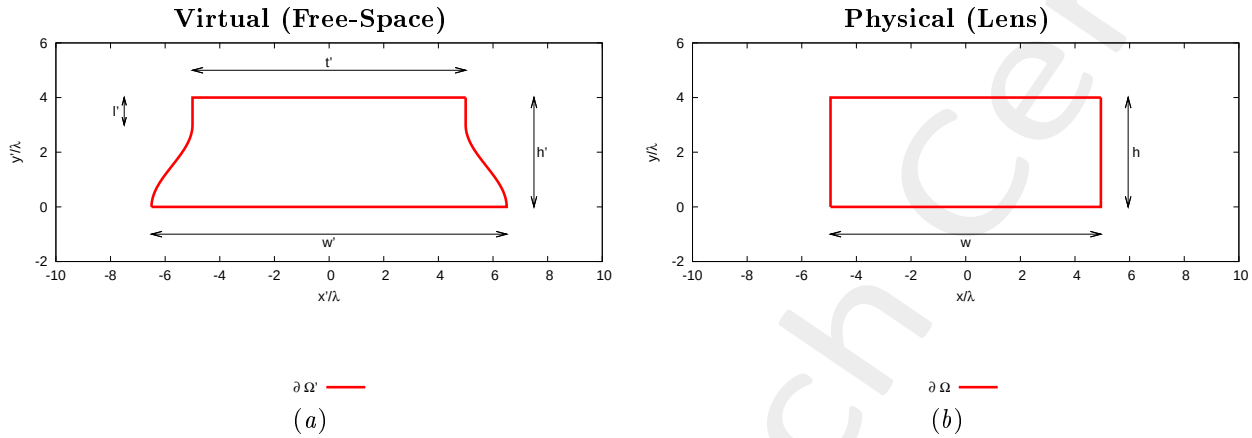

Figure 1: Transformation regions. The lower side of both virtual and physical boundaries are supposed to be PEC.

- **Virtual Geometry**

# Test Case	h' [λ]	l' [λ]	t' [λ]	w' [λ]
1	4.0	1.0	10.0	**11.0**
2	4.0	1.0	10.0	**11.7**
3	4.0	1.0	10.0	**12.4**
4	4.0	1.0	10.0	**13.0**
5	4.0	1.0	10.0	**13.6**

Table I: Considered virtual geometries. The values of w' have been empirically determined in order to achieve an aperture of the virtual array (L') equal to a multiple of $\lambda/2$. It is imposed that $h = h'$, while w is not controlled by the user.

- **Physical Array**
  - Number of elements, spacing, aperture: $N = 15$, $d = \frac{\lambda}{2}$, $L = 7.0$ [λ];
  - Positions: $x_n \in [-L/2, L/2]$, $y_n = \frac{\lambda}{4}$, $n = 1, ..., N$;
  - Steering angle: $\phi_s = 90.0$ [deg];
  - Excitations: $I_n = 1.0$, $\varphi_n = \frac{-2\pi}{\lambda} x_n sin\,(\phi_s + 90)$; $n = 1, ..., N$;
- **QCTO**
  - Discretization cell dimension: 0.15 [λ] (0.01 [λ] for source mapping);

1.1.1 Results

Transformation grids

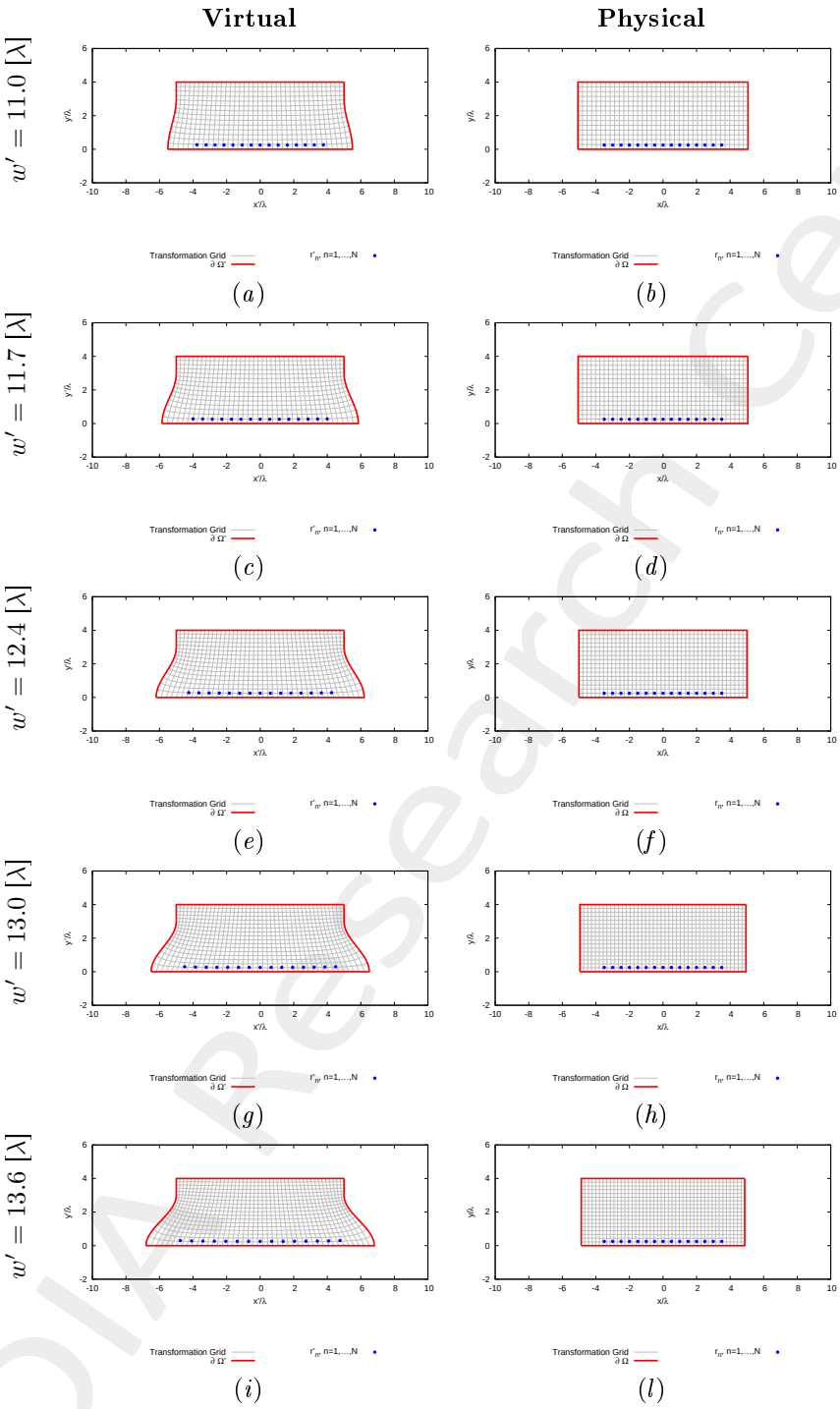

Figure 2: Transformation grids for different values of w'. Physical geometry has been shifted on y by $h/2 = 2.0$ $[\lambda]$.

Resulting aperture of the virtual array (L') - for step 2

- The aperture of the virtual array (L') is computed after mapping the physical array into the virtual space;
- The resulting number of equi-spaced elements is computed as

$$N' = round\left(\frac{L'}{0.5} + 1\right)$$

	Virtual Geometry				**Virtual Array**	
# Test Case	h' [λ]	l' [λ]	t' [λ]	w' [λ]	L' [λ]	N'
1	4.0	1.0	10.0	**11.0**	7.54	**16**
2	4.0	1.0	10.0	**11.7**	8.00	**17**
3	4.0	1.0	10.0	**12.4**	8.51	**18**
4	4.0	1.0	10.0	**13.0**	8.99	**19**
5	4.0	1.0	10.0	**13.6**	9.52	**20**

Table II: Resulting aperture and number of equi-spaced elements of the virtual array after expanding the physical array.

1.2 Step 2: Compressing the virtual array ($N' > N$, $L' > L$ [λ])

Input Parameters

- **Virtual Array**
  - Number of elements, spacing, aperture: $N' = \{16; 17; 18; 19; 20\}$, $d' = \frac{\lambda}{2}$, $L' = \{7.5; 8.0; 8.5; 9.0; 9.5\}$ $[\lambda]$;
  - Positions: $x'_n \in [-L'/2, L'/2]$, $y'_n = \lambda/4$, $n = 1, ..., N'$;
  - Steering angle: $\phi_s = 90.0$ $[deg]$;
  - Excitations: $I'_n = 1.0$, $\varphi'_n = \frac{-2\pi}{\lambda} x_n sin\,(\phi_s + 90)$; $n = 1, ..., N'$;
- **Virtual Geometry:** same of step 1;
- **QCTO:** same of step 1.

1.2.1 Results of the Transformation

Transformation grids

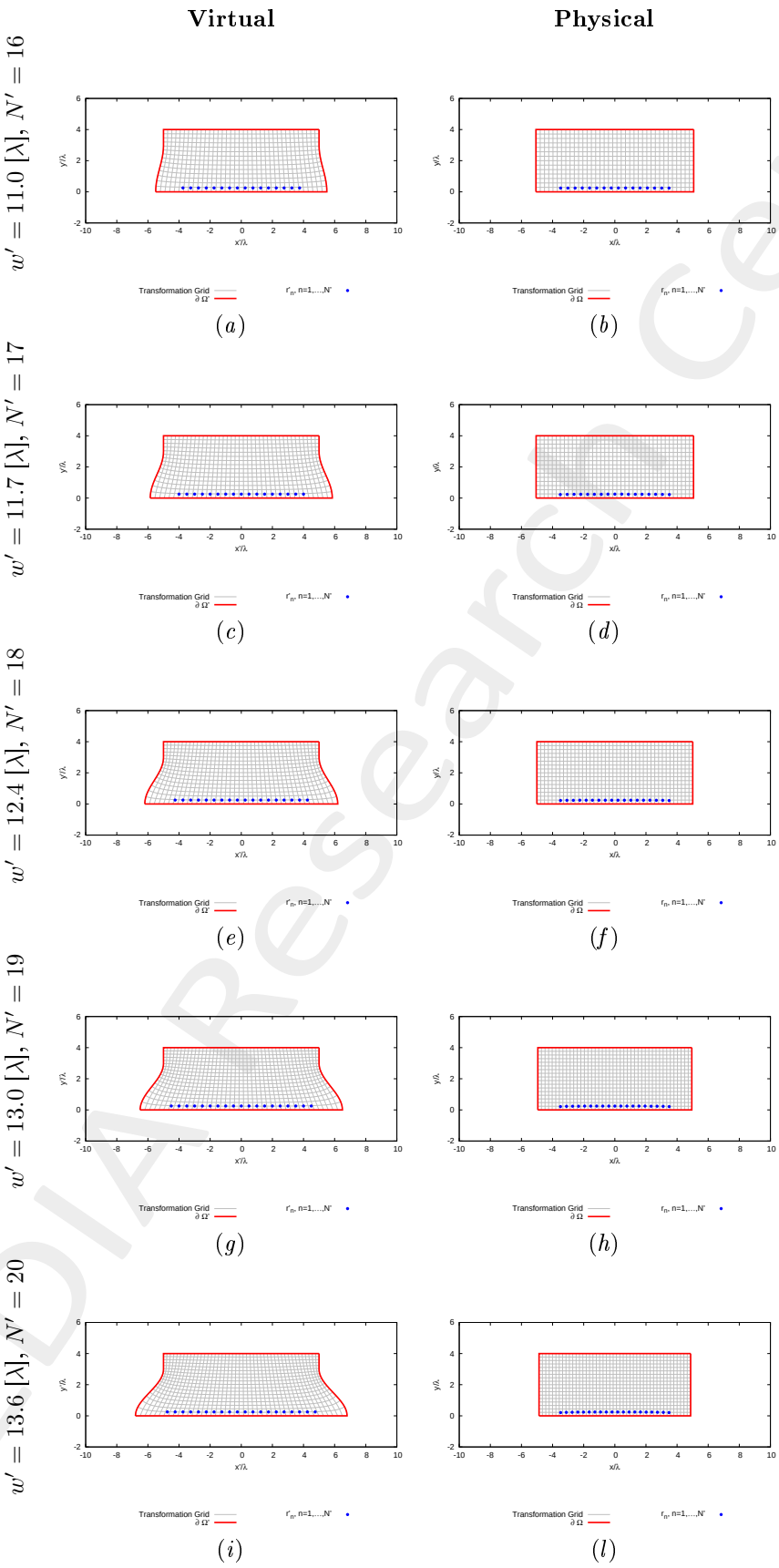

Figure 3: Transformation grids for different values of w'. Physical geometry has been shifted on y by $h/2 = 2.0$ $[\lambda]$.

Lens Permittivity - $w' = 11.0\ [\lambda]$

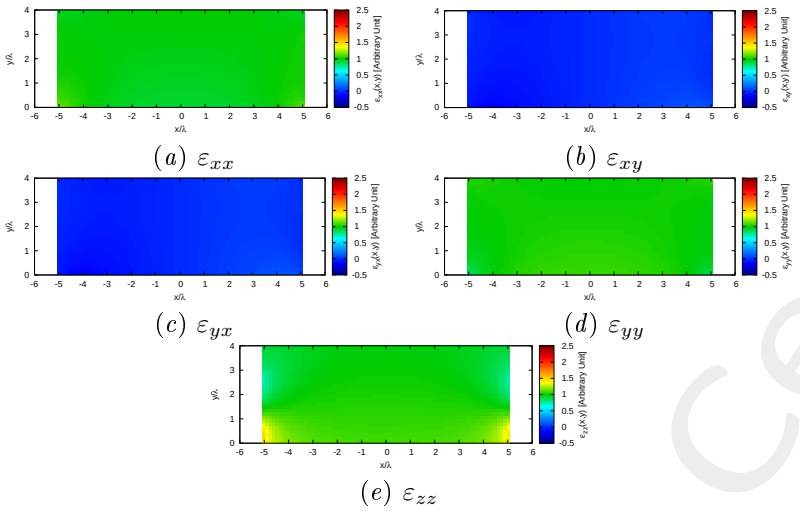

Figure 4: Components of the relative permittivity tensor of the lens.

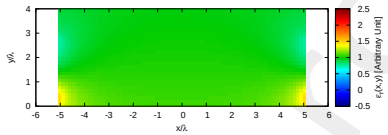

Figure 5: Isotropic approximate permittivity distribution of the lens.

Lens Permittivity - $w' = 11.7\ [\lambda]$

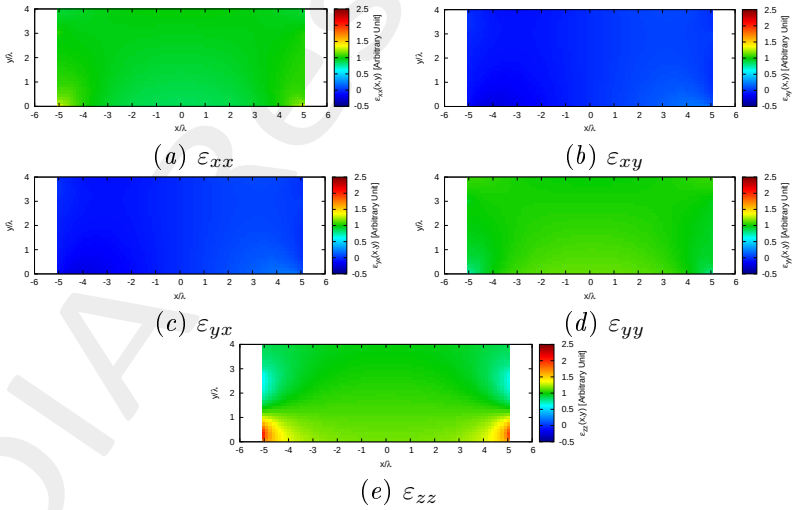

Figure 6: Components of the relative permittivity tensor of the lens.

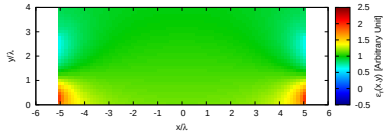

Figure 7: Isotropic approximate permittivity distribution of the lens.

Lens Permittivity - $w' = 12.4\ [\lambda]$

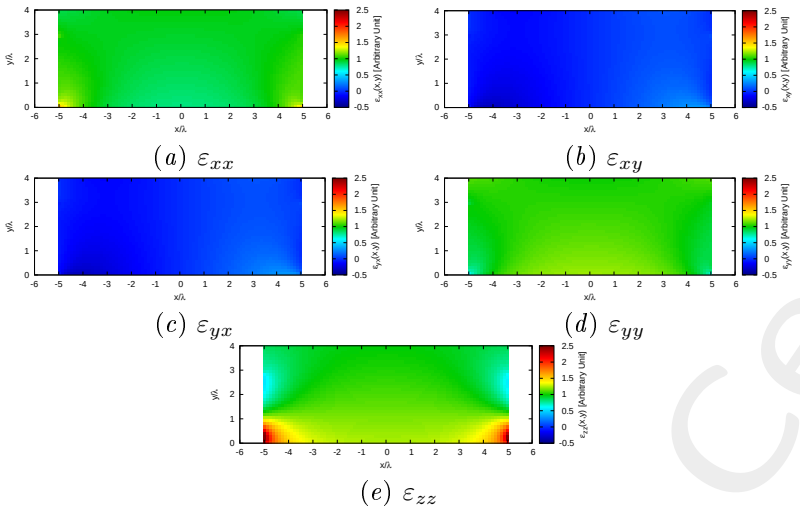

Figure 8: Components of the relative permittivity tensor of the lens.

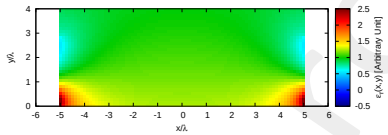

Figure 9: Isotropic approximate permittivity distribution of the lens.

Lens Permittivity - $w' = 13.0\ [\lambda]$

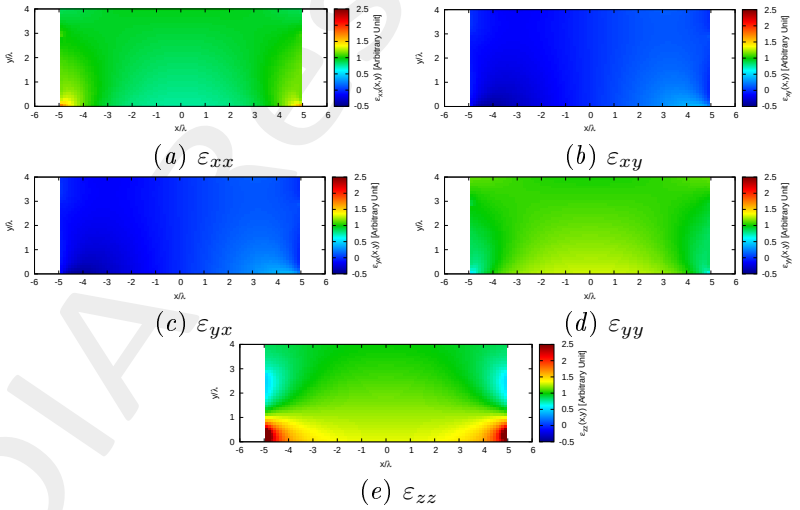

Figure 10: Components of the relative permittivity tensor of the lens.

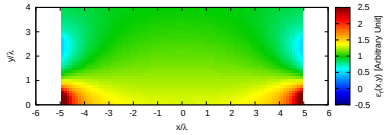

Figure 11: Isotropic approximate permittivity distribution of the lens.

Lens Permittivity - $w' = 13.6\ [\lambda]$

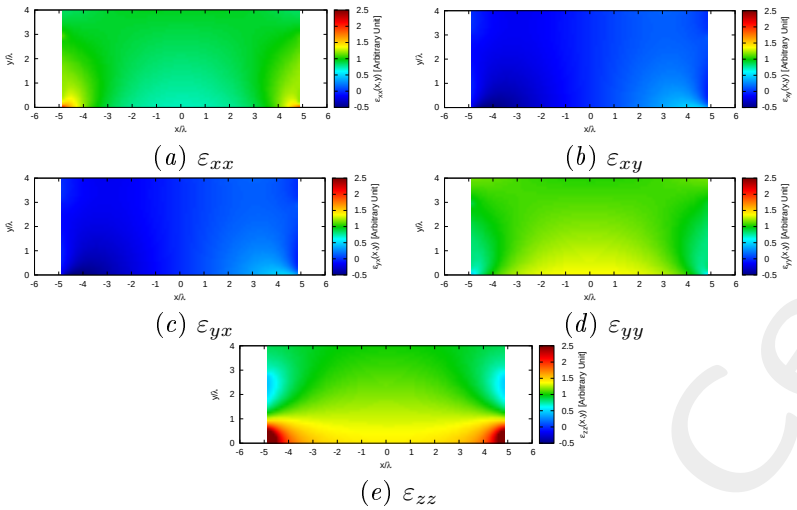

(a) ε_{xx} (b) ε_{xy} (c) ε_{yx} (d) ε_{yy} (e) ε_{zz}

Figure 12: Components of the relative permittivity tensor of the lens.

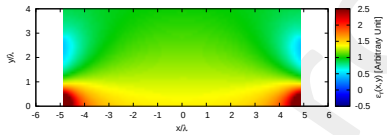

Figure 13: Isotropic approximate permittivity distribution of the lens.

Physical Lens Parameters

Parameter	$w' = 11.0\ [\lambda]$	$w' = 11.7\ [\lambda]$	$w' = 12.4\ [\lambda]$	$w' = 13.0\ [\lambda]$	$w' = 13.6\ [\lambda]$
Height, $h\ [\lambda]$	4.00	4.00	4.00	4.00	4.00
Width, $w\ [\lambda]$	10.14	10.12	10.12	9.89	9.74
Anisotropic Permittivity Range	$[-0.12, 1.49]$	$[-0.22, 2.01]$	$[-0.32, 2.72]$	$[-0.41, 3.56]$	$[-0.50, 4.61]$
Isotropic Permittivity Range	$[0.00, 1.47]$	$[0.00, 1.96]$	$[0.00, 2.66]$	$[0.00, 3.44]$	$[0.00, 4.40]$
Average Fractional Anisotropy, α_F	6.29×10^{-2}	1.08×10^{-1}	1.52×10^{-1}	1.89×10^{-1}	2.25×10^{-1}
Average Relative Anisotropy, α_R	5.20×10^{-2}	9.02×10^{-2}	1.30×10^{-1}	1.64×10^{-1}	1.99×10^{-1}

Table III: Transformation statistics. Note that we impose $h = h'$, while w is internally chosen by the QCTO software.

Virtual Grid Orthogonality

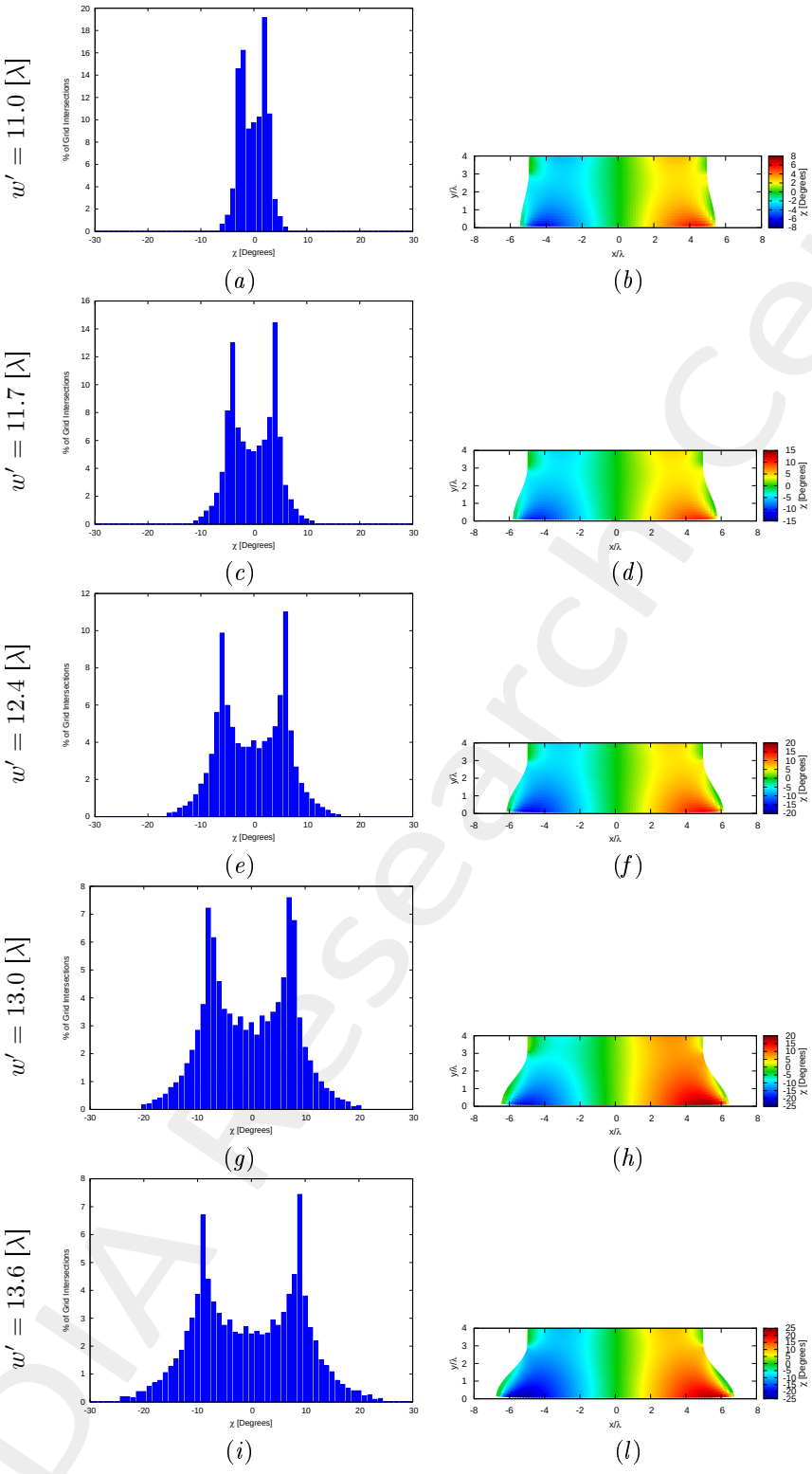

Figure 14: Orthogonality of the virtual grid for different values of w'.

1.2.2 Near-Field Distributions ($\phi_s = 90$ [deg], $f = 600$ [MHz])

Case $w' = 11.0$ [λ], $N' = 16$

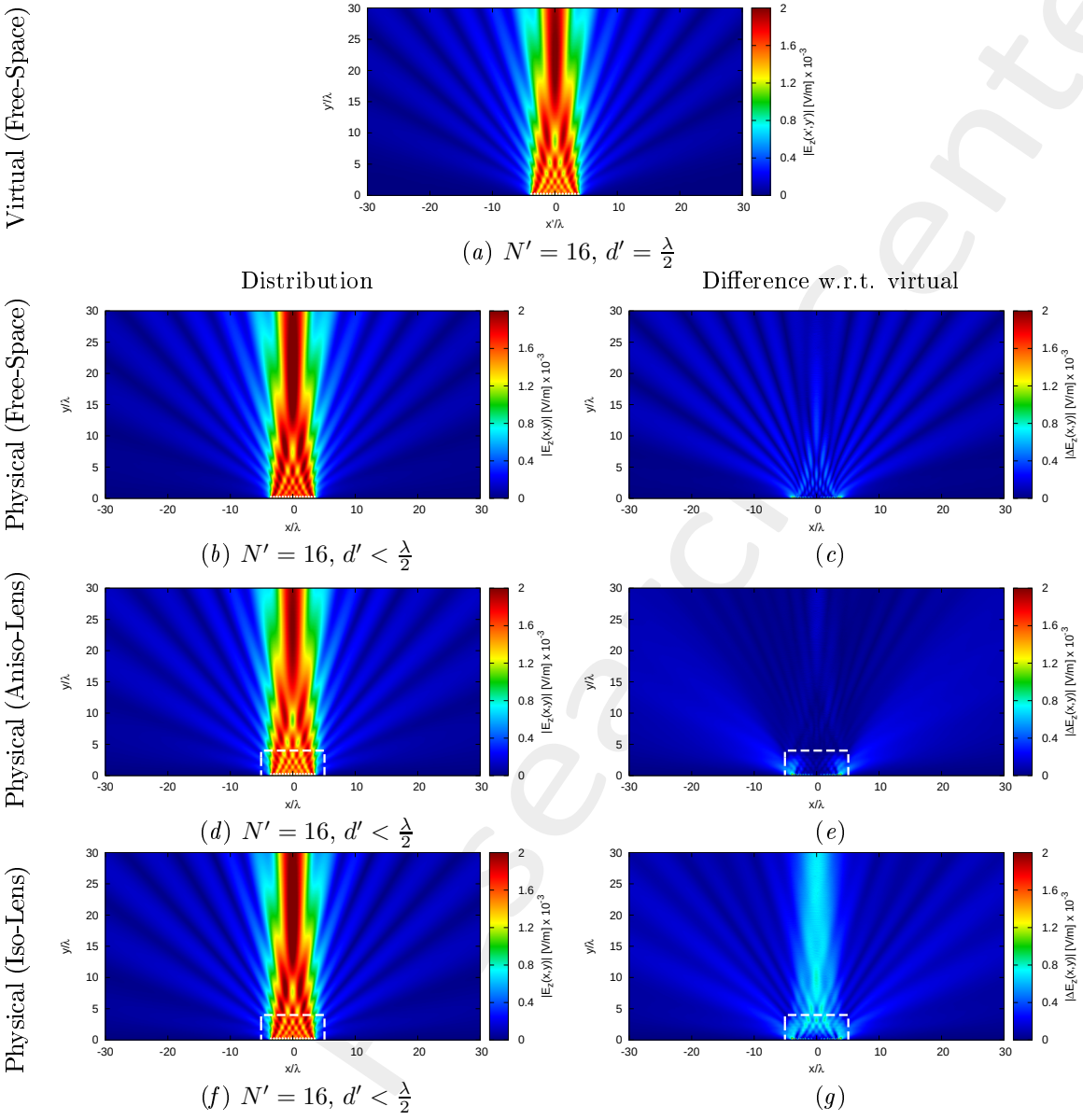

(a) $N' = 16$, $d' = \frac{\lambda}{2}$

(b) $N' = 16$, $d' < \frac{\lambda}{2}$ (c)

(d) $N' = 16$, $d' < \frac{\lambda}{2}$ (e)

(f) $N' = 16$, $d' < \frac{\lambda}{2}$ (g)

Figure 15: Electric field distributions.

Case $w' = 11.7$ **[**λ**],** $N' = 17$

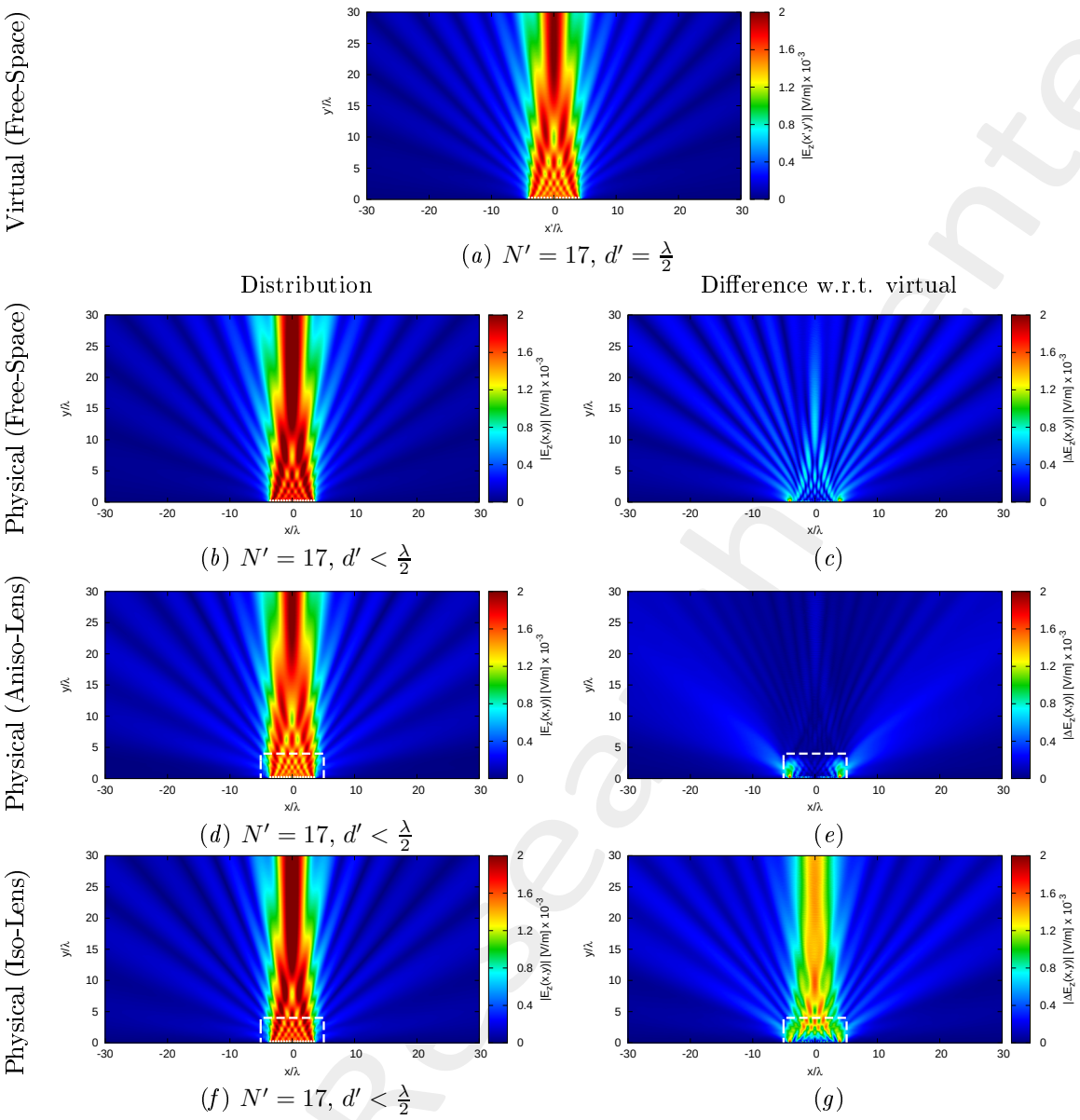

(a) $N' = 17$, $d' = \frac{\lambda}{2}$

(b) $N' = 17$, $d' < \frac{\lambda}{2}$ (c)

(d) $N' = 17$, $d' < \frac{\lambda}{2}$ (e)

(f) $N' = 17$, $d' < \frac{\lambda}{2}$ (g)

Figure 16: Electric field distributions.

Case $w' = 12.4$ **[**λ**],** $N' = 18$

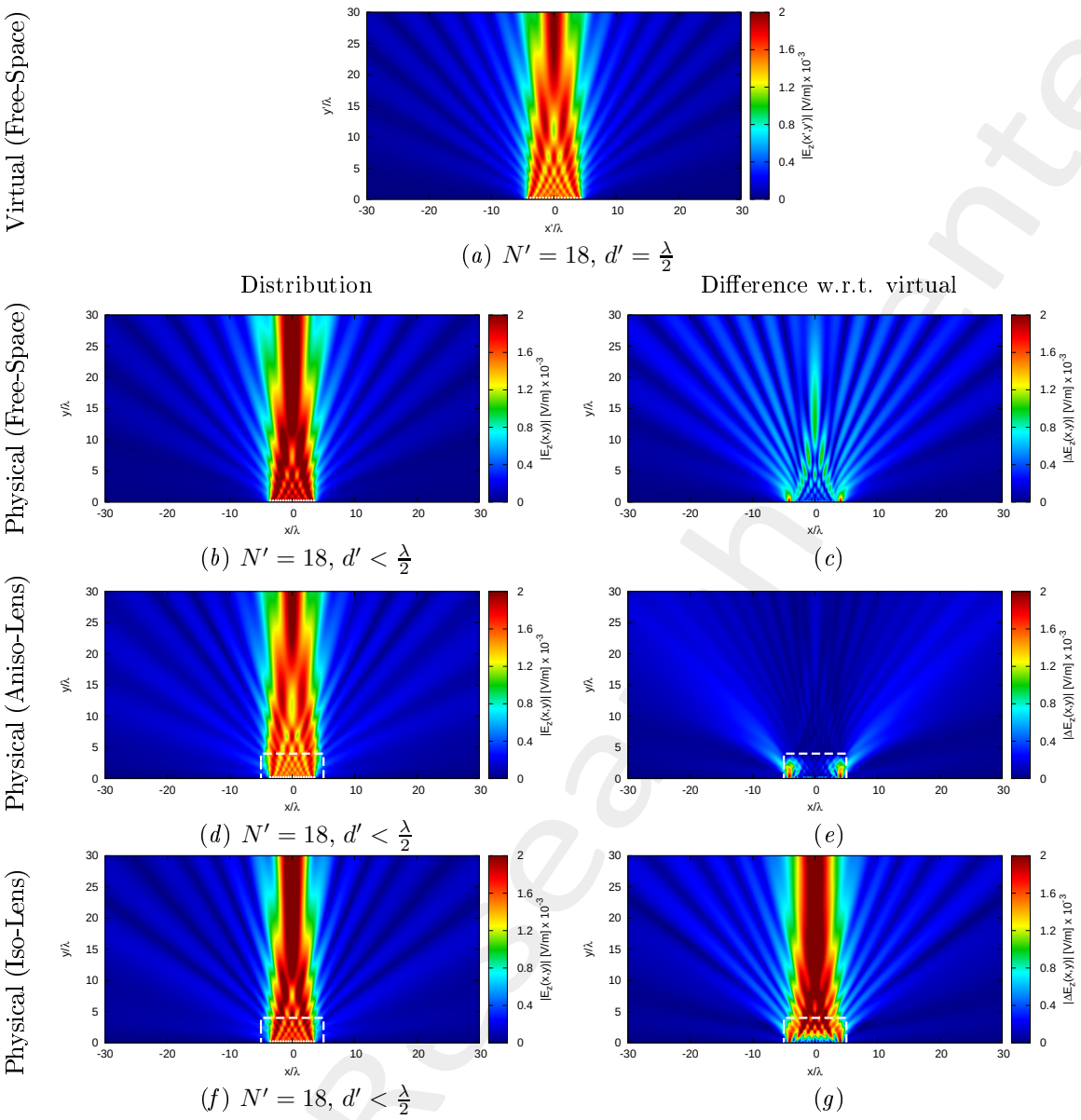

(a) $N' = 18$, $d' = \frac{\lambda}{2}$

(b) $N' = 18$, $d' < \frac{\lambda}{2}$ (c)

(d) $N' = 18$, $d' < \frac{\lambda}{2}$ (e)

(f) $N' = 18$, $d' < \frac{\lambda}{2}$ (g)

Figure 17: Electric field distributions.

Case $w' = 13.0$ **[**λ**],** $N' = 19$

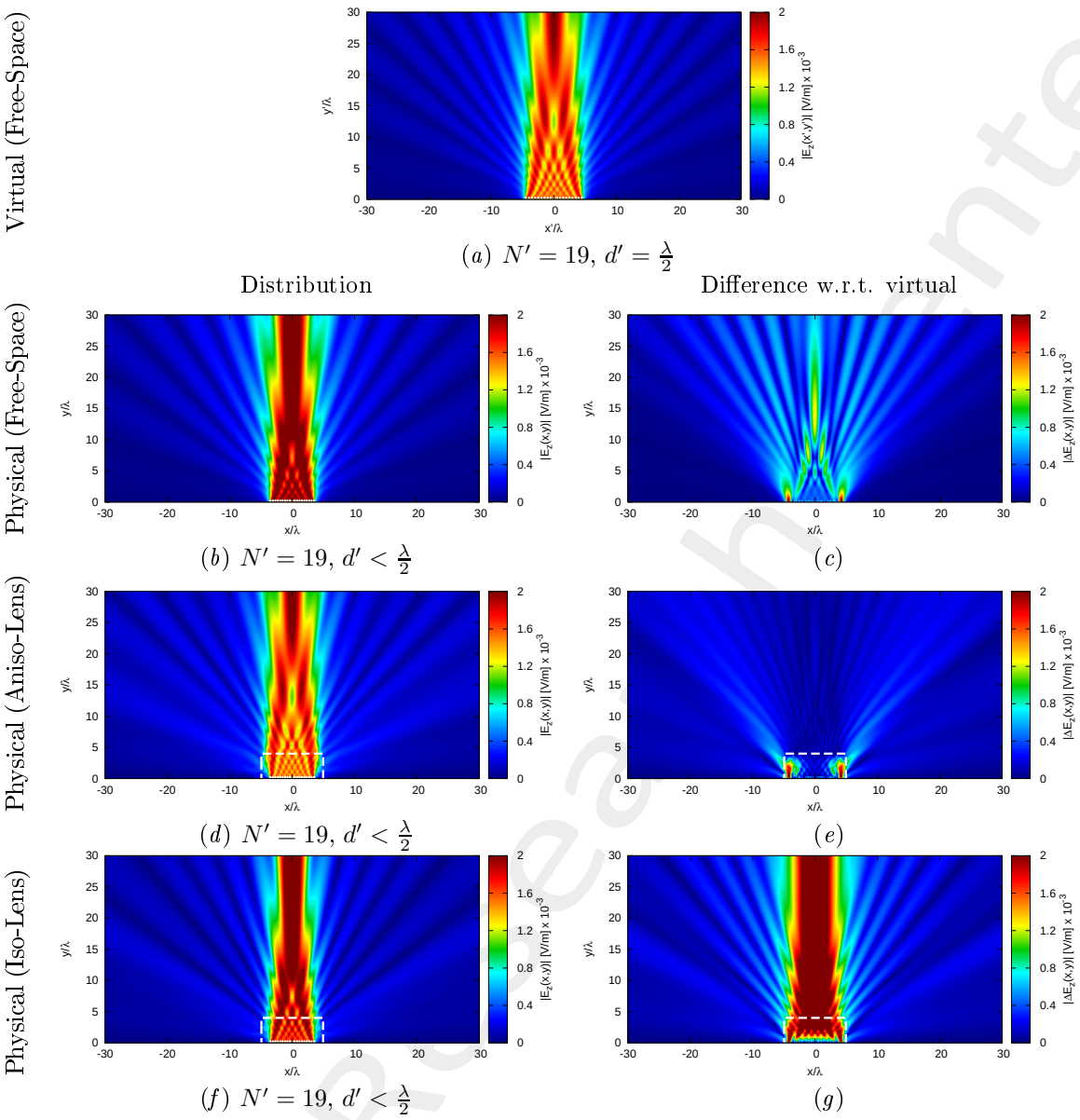

(a) $N' = 19$, $d' = \frac{\lambda}{2}$

(b) $N' = 19$, $d' < \frac{\lambda}{2}$ (c)

(d) $N' = 19$, $d' < \frac{\lambda}{2}$ (e)

(f) $N' = 19$, $d' < \frac{\lambda}{2}$ (g)

Figure 18: Electric field distributions.

Case $w' = 13.6$ **[**λ**],** $N' = 20$

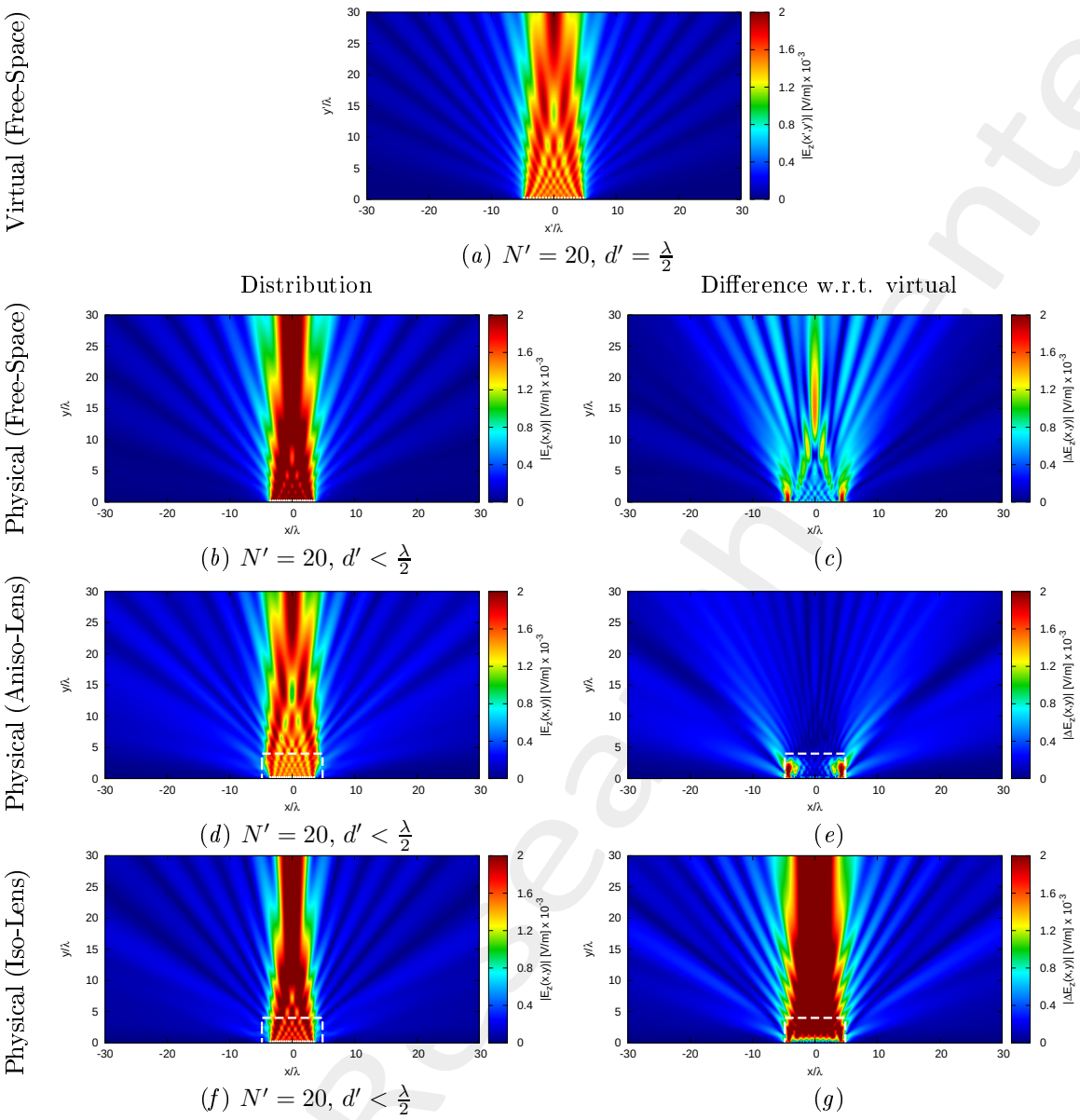

(a) $N' = 20$, $d' = \frac{\lambda}{2}$

(b) $N' = 20$, $d' < \frac{\lambda}{2}$ (c)

(d) $N' = 20$, $d' < \frac{\lambda}{2}$ (e)

(f) $N' = 20$, $d' < \frac{\lambda}{2}$ (g)

Figure 19: Electric field distributions.

1.2.3 Far-Field Patterns ($\phi_s = 90$ [deg], $f = 600$ [MHz])

Anisotropic Lens

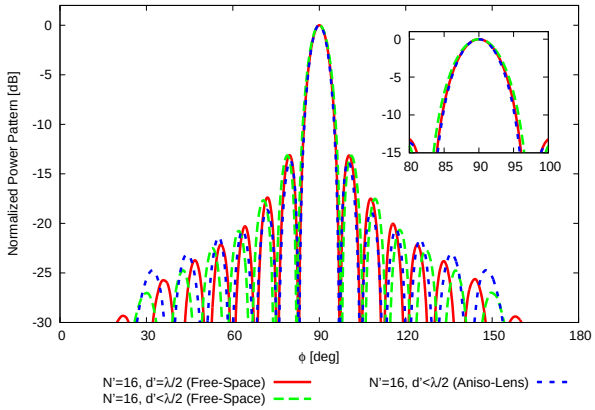

(a) $w' = 11.0$ $[\lambda]$, $N' = 16$

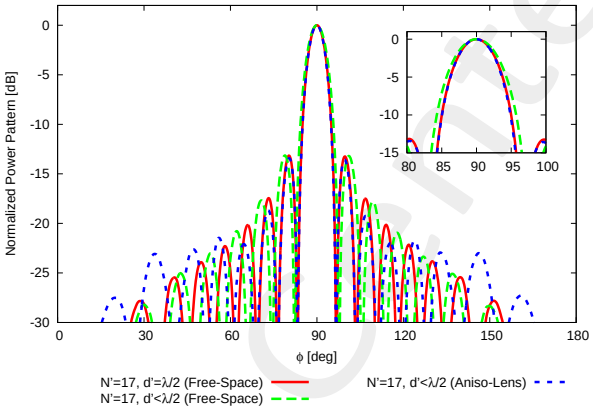

(b) $w' = 11.7$ $[\lambda]$, $N' = 17$

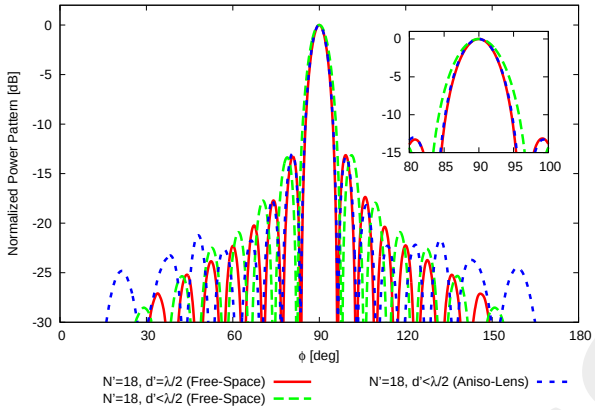

(c) $w' = 12.4$ $[\lambda]$, $N' = 18$

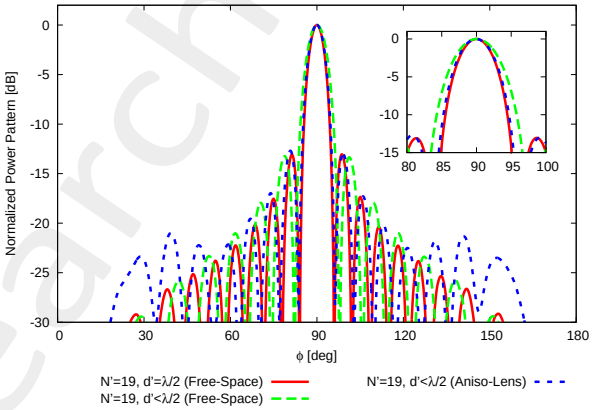

(d) $w' = 13.0$ $[\lambda]$, $N' = 19$

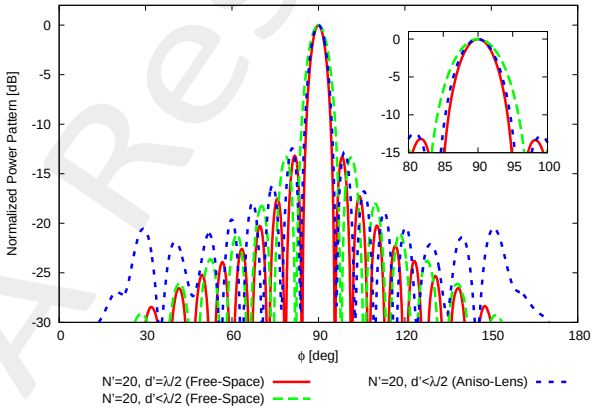

(e) $w' = 13.6$ $[\lambda]$, $N' = 20$

Figure 20: Far field pattern comparison for different values of w'.

Isotropic Lens

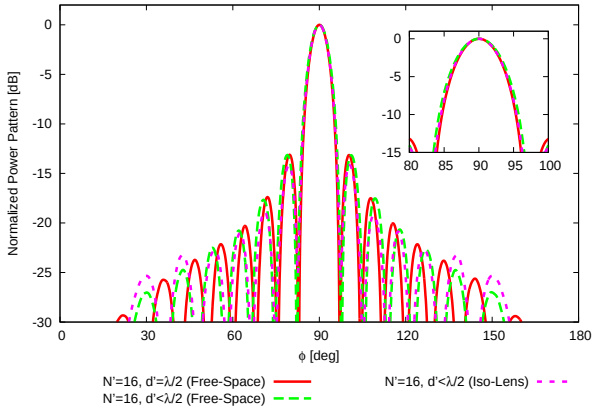

(a) $w' = 11.0$ $[\lambda]$, $N' = 16$

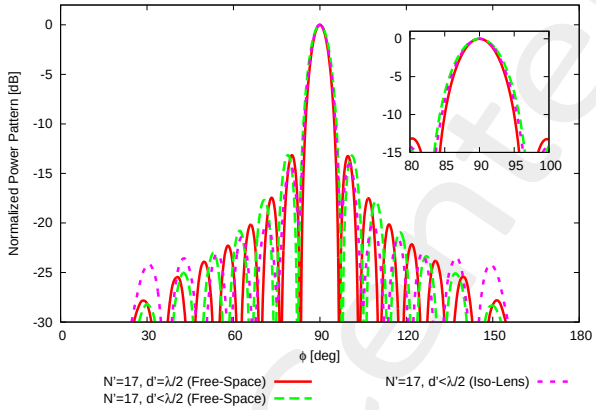

(b) $w' = 11.7$ $[\lambda]$, $N' = 17$

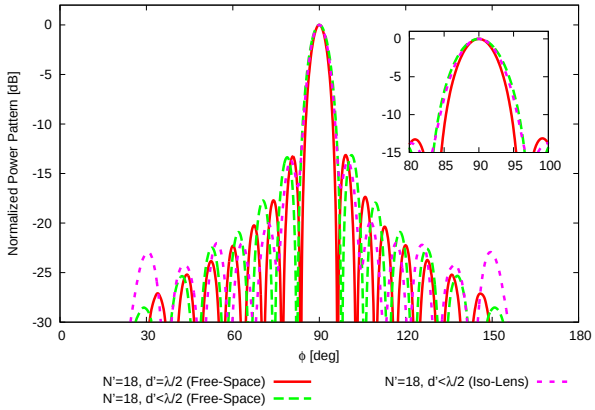

(c) $w' = 12.4$ $[\lambda]$, $N' = 18$

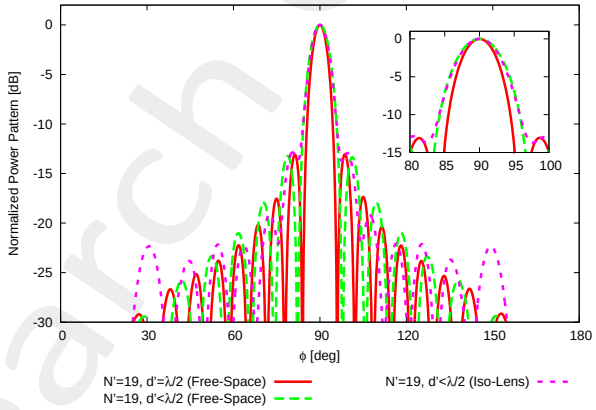

(d) $w' = 13.0$ $[\lambda]$, $N' = 19$

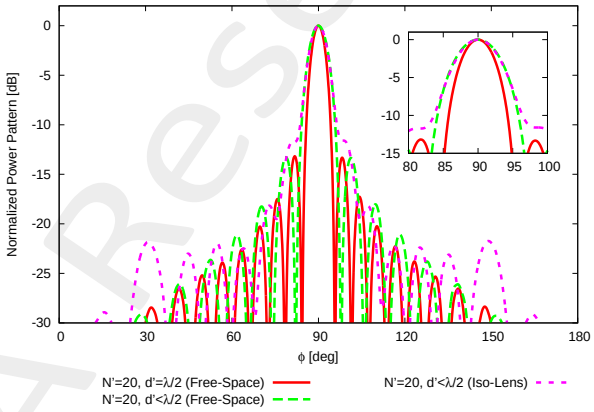

(e) $w' = 13.6$ $[\lambda]$, $N' = 20$

Figure 21: Far field pattern comparison for different values of w'.

1.2.4 Summary ($\phi_s = 90$ [deg], $f = 600$ [MHz])

$w' = 11.0$ [λ]				
	Virtual Array	**Physical Array**		
Environment	Free-Space	Free-Space	Aniso-Lens	Iso-Lens
Number of elements	16	16		
Spacing [λ]	0.5	< 0.5		
Aperture [λ]	7.5	6.97		
SLL [dB]	13.11	13.14	13.67	14.18
$FNBW$ [deg]	14.32	15.40	14.05	14.86
3dB Beamwidth [deg]	6.36	6.83	6.16	6.45
Matching Error, ξ (w.r.t. virtual, outside lens)	-	3.66×10^{-1}	3.02×10^{-1}	5.98×10^{-1}
$w' = 11.7$ [λ]				
	Virtual Array	**Physical Array**		
Environment	Free-Space	Free-Space	Aniso-Lens	Iso-Lens
Number of elements	17	17		
Spacing [λ]	0.5	< 0.5		
Aperture [λ]	8.0	7.00		
SLL [dB]	13.16	13.15	13.43	14.08
$FNBW$ [deg]	13.60	15.40	13.42	14.68
3dB Beamwidth [deg]	5.97	6.84	5.88	6.35
Matching Error, ξ (w.r.t. virtual, outside lens)	-	5.89×10^{-1}	3.98×10^{-1}	9.18×10^{-1}
$w' = 12.4$ [λ]				
	Virtual Array	**Physical Array**		
Environment	Free-Space	Free-Space	Aniso-Lens	Iso-Lens
Number of elements	18	18		
Spacing [λ]	0.5	< 0.5		
Aperture [λ]	8.5	6.98		
SLL [dB]	13.14	13.14	13.00	13.73
$FNBW$ [deg]	12.79	15.58	12.97	14.86
3dB Beamwidth [deg]	5.64	6.89	5.75	6.43
Matching Error, ξ (w.r.t. virtual, outside lens)	-	7.04×10^{-1}	4.13×10^{-1}	1.17
$w' = 13.0$ [λ]				
	Virtual Array	**Physical Array**		
Environment	Free-Space	Free-Space	Aniso-Lens	Iso-Lens
Number of elements	19	19		
Spacing [λ]	0.5	< 0.5		
Aperture [λ]	9.0	6.99		
SLL [dB]	13.06	13.24	12.69	12.87
$FNBW$ [deg]	12.07	15.67	12.70	15.22
3dB Beamwidth [deg]	5.35	6.87	5.64	6.54
Matching Error, ξ (w.r.t. virtual, outside lens)	-	6.93×10^{-1}	4.83×10^{-1}	1.42
$w' = 13.6$ [λ]				
	Virtual Array	**Physical Array**		
Environment	Free-Space	Free-Space	Aniso-Lens	Iso-Lens
Number of elements	20	20		
Spacing [λ]	0.5	< 0.5		
Aperture [λ]	9.5	6.96		
SLL [dB]	13.18	13.29	12.45	11.60
$FNBW$ [deg]	11.44	15.76	12.52	16.66
3dB Beamwidth [deg]	5.06	6.98	5.58	6.78
Matching Error, ξ (w.r.t. virtual, outside lens)	-	7.24×10^{-1}	5.79×10^{-1}	1.60

Table IV: Summary for step 2.

1.3 Source Inversion (SI)

Parameters

- Before SI
  - Number of elements: $N' = \{16; 17; 18; 19; 20\}$, $d' < \lambda/2$;
- After SI
  - Number of elements after SI: $N = 15$, $d = \frac{\lambda}{2}$;
  - Aperture: $L = 7.0$;
- Radius of the observation domain: $r_{SI} = 50.0$ $[\lambda]$;
- Number of field sampling points: $n_{SI} = 1000$.

1.3.1 Results of the SI ($\phi_s = 90$ [deg], $f = 600$ [MHz])

Synthesized Excitations

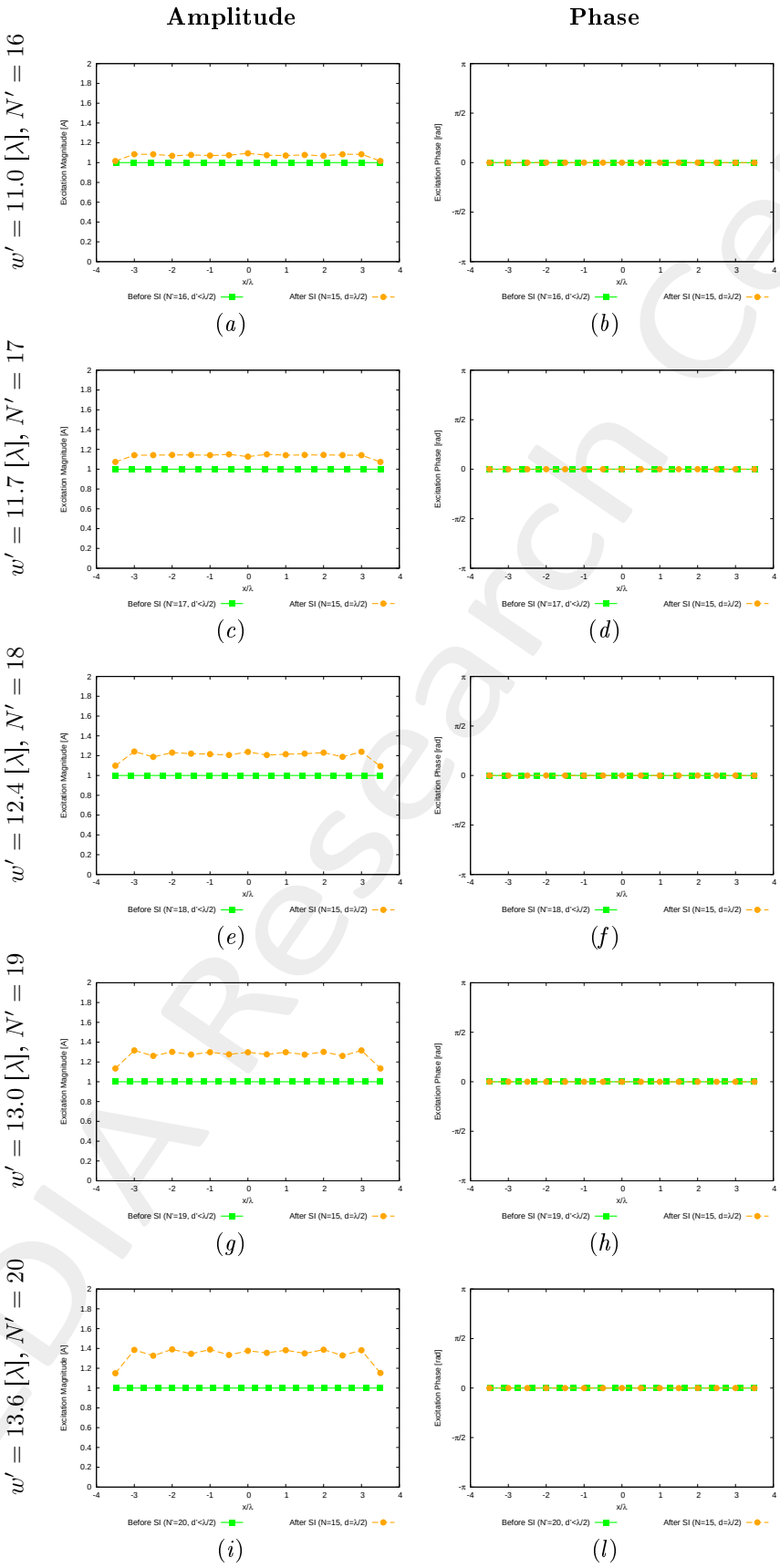

Figure 22: $\phi_s = 90$ [deg], $f = 600$ [MHz] - Synthesized excitations through SI.

Check SI: Free-Space Patterns

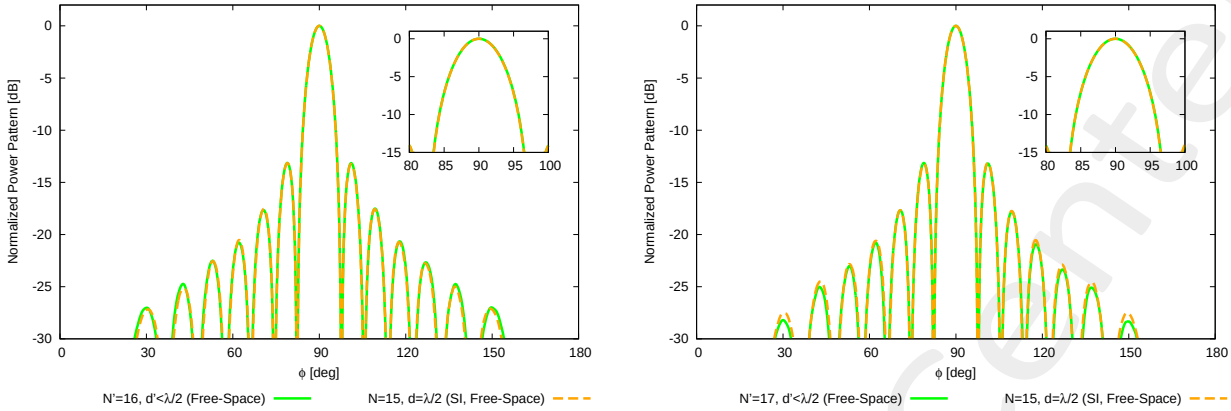

(a) $w' = 11.0$ $[\lambda]$, $N' = 16$

(b) $w' = 11.7$ $[\lambda]$, $N' = 17$

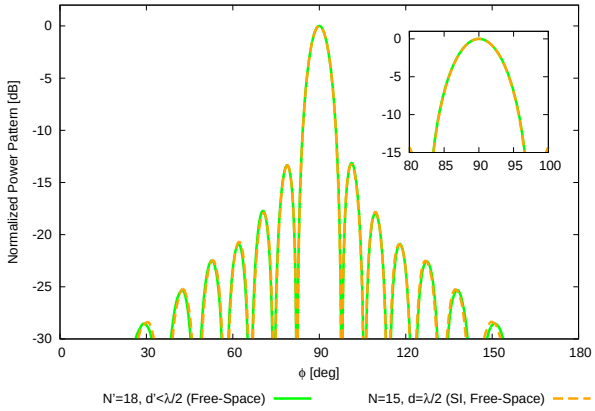

(c) $w' = 12.4$ $[\lambda]$, $N' = 18$

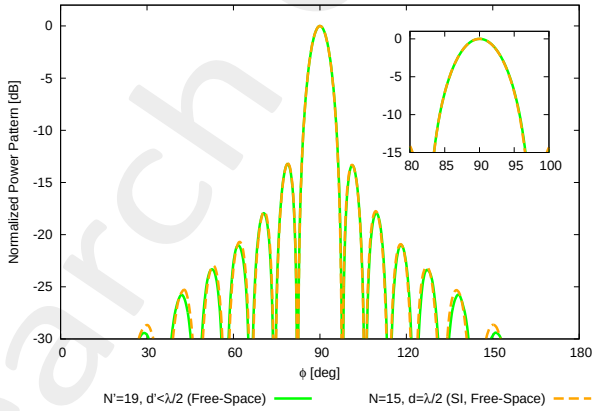

(d) $w' = 13.0$ $[\lambda]$, $N' = 19$

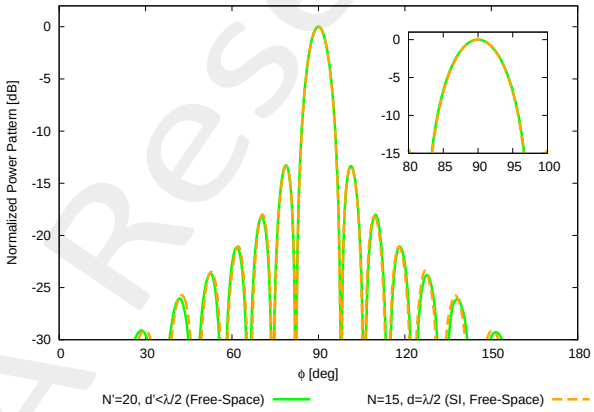

(e) $w' = 13.6$ $[\lambda]$, $N' = 20$

Figure 23: $\phi_s = 90$ [deg], $f = 600$ [MHz] - Free-space far field pattern comparison for different values of w'.

1.3.2 Near-Field Distribution ($\phi_s = 90$ [deg], $f = 600$ [MHz])

Case $w' = 11.0$ [λ], $N' = 16$

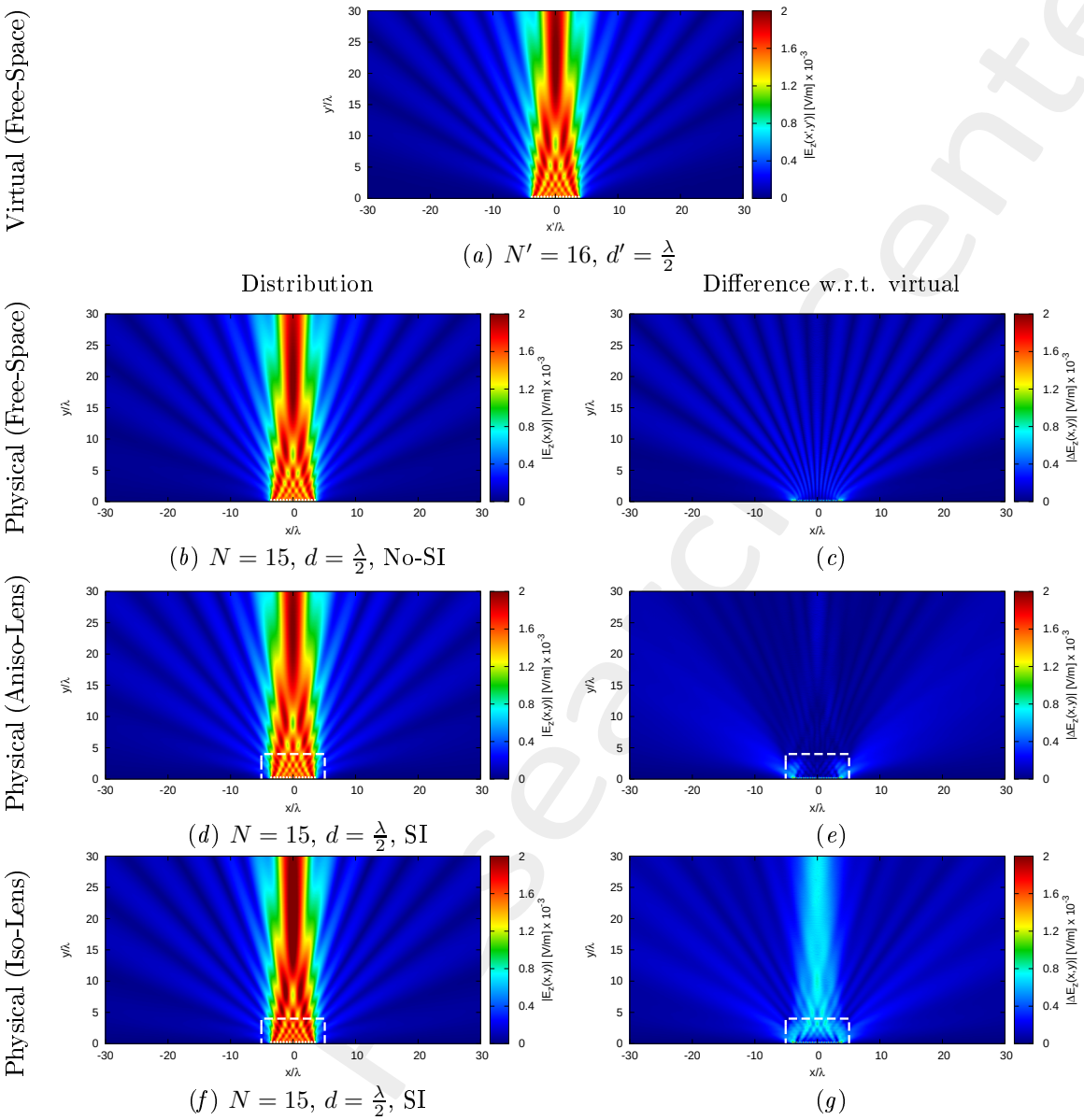

(a) $N' = 16$, $d' = \frac{\lambda}{2}$

(b) $N = 15$, $d = \frac{\lambda}{2}$, No-SI (c)

(d) $N = 15$, $d = \frac{\lambda}{2}$, SI (e)

(f) $N = 15$, $d = \frac{\lambda}{2}$, SI (g)

Figure 24: $\phi_s = 90$ [deg], $f = 600$ [MHz] - Electric field distributions.

Case $w' = 11.7$ **[**λ**],** $N' = 17$

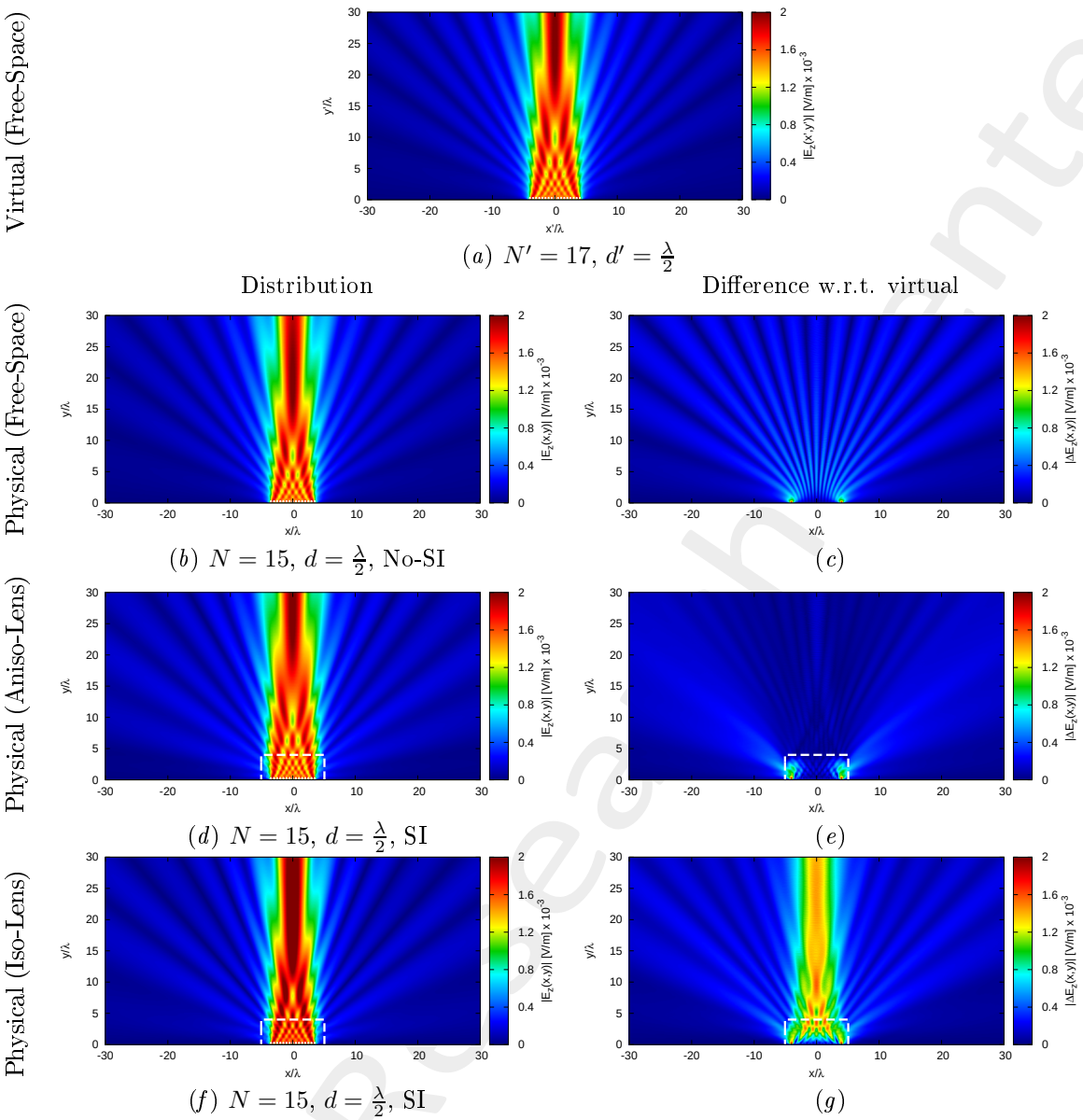

(a) $N' = 17$, $d' = \frac{\lambda}{2}$

(b) $N = 15$, $d = \frac{\lambda}{2}$, No-SI (c)

(d) $N = 15$, $d = \frac{\lambda}{2}$, SI (e)

(f) $N = 15$, $d = \frac{\lambda}{2}$, SI (g)

Figure 25: $\phi_s = 90$ [deg], $f = 600$ [MHz] - Electric field distributions.

Case $w' = 12.4$ **[**λ**],** $N' = 18$

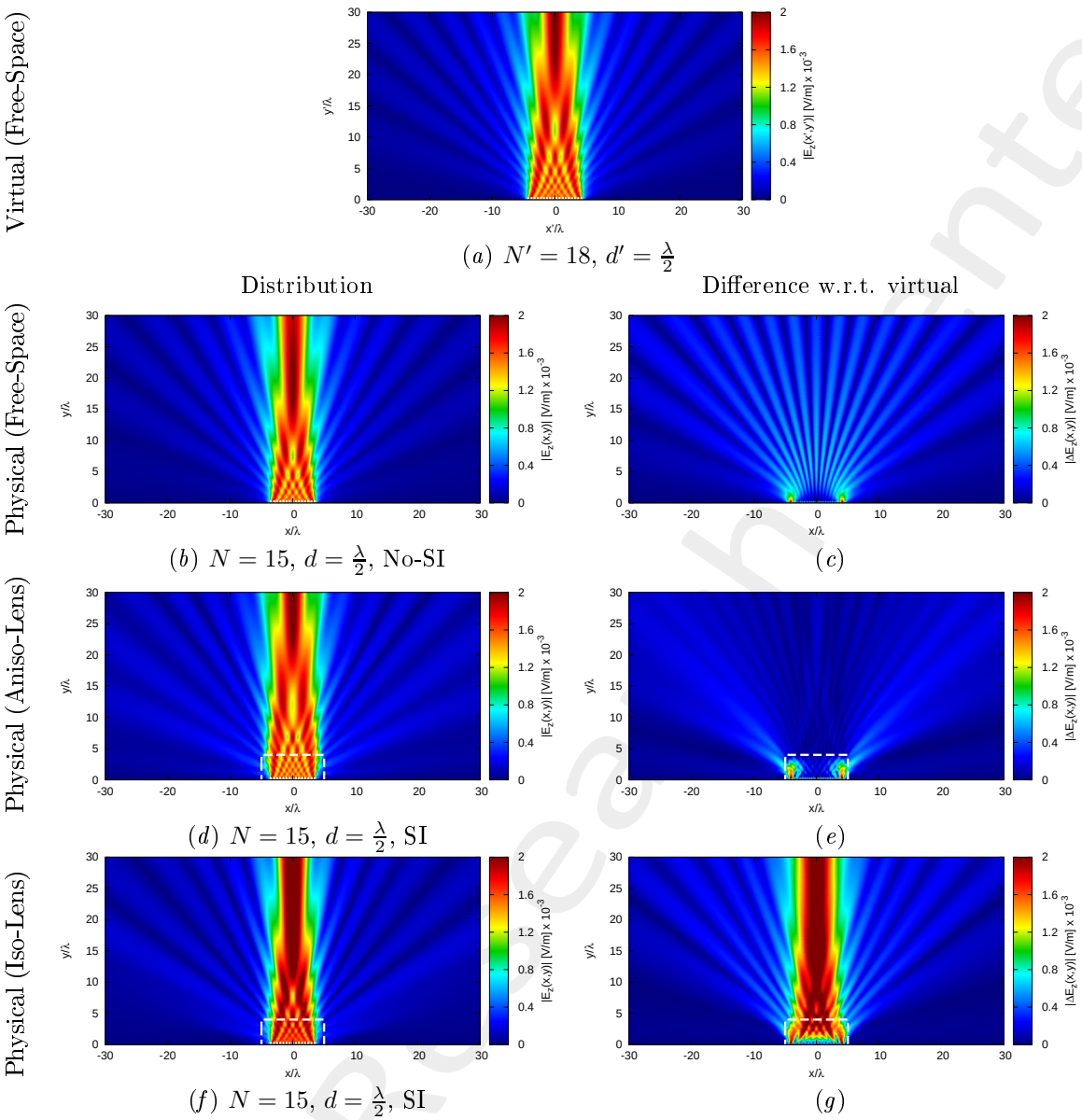

(a) $N' = 18$, $d' = \frac{\lambda}{2}$

(b) $N = 15$, $d = \frac{\lambda}{2}$, No-SI (c)

(d) $N = 15$, $d = \frac{\lambda}{2}$, SI (e)

(f) $N = 15$, $d = \frac{\lambda}{2}$, SI (g)

Figure 26: $\phi_s = 90$ [deg], $f = 600$ [MHz] - Electric field distributions.

Case $w' = 13.0$ **[**λ**],** $N' = 19$

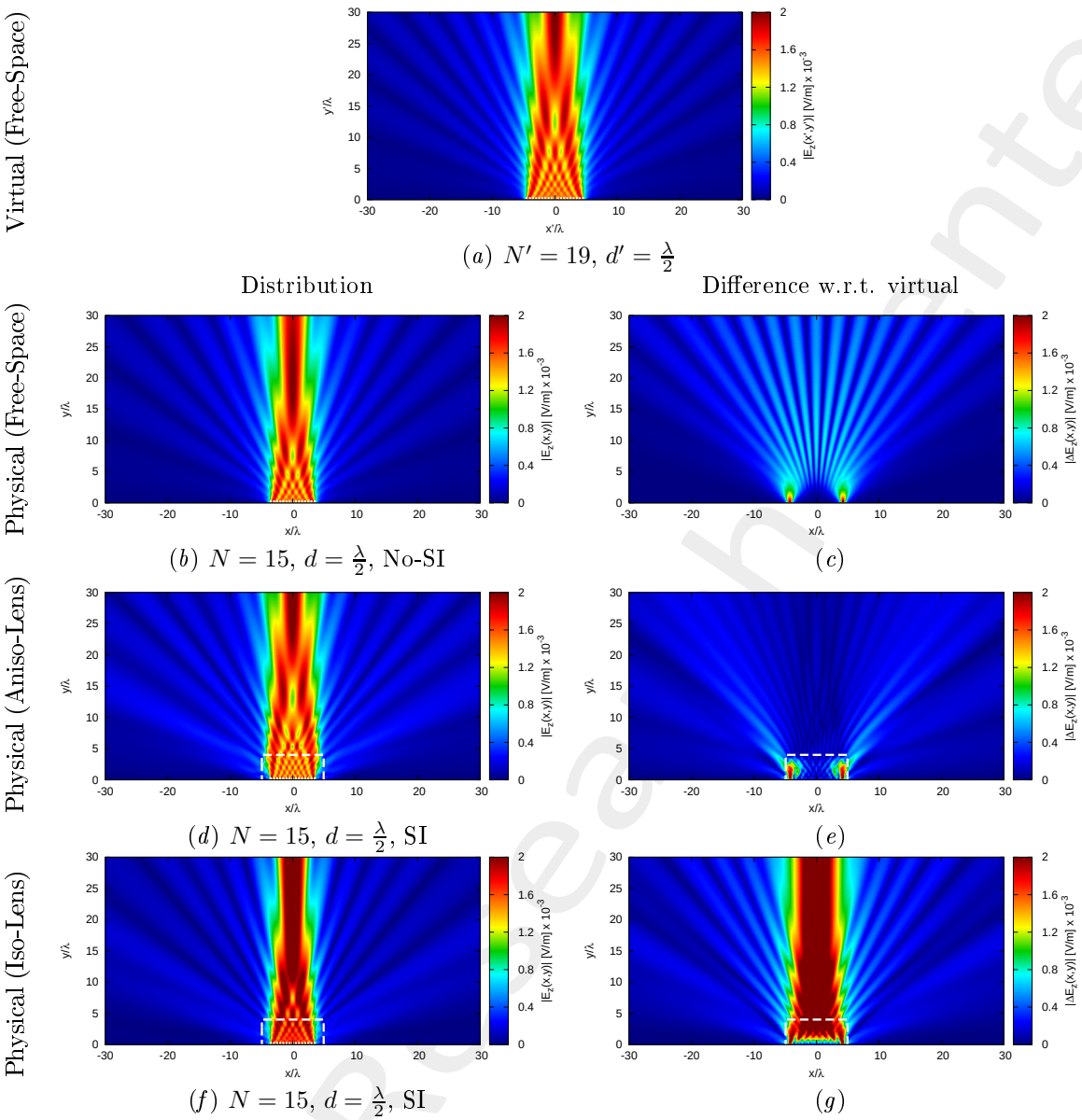

(a) $N' = 19$, $d' = \frac{\lambda}{2}$

(b) $N = 15$, $d = \frac{\lambda}{2}$, No-SI (c)

(d) $N = 15$, $d = \frac{\lambda}{2}$, SI (e)

(f) $N = 15$, $d = \frac{\lambda}{2}$, SI (g)

Figure 27: $\phi_s = 90$ [deg], $f = 600$ [MHz] - Electric field distributions.

Case $w' = 13.6$ **[**λ**],** $N' = 20$

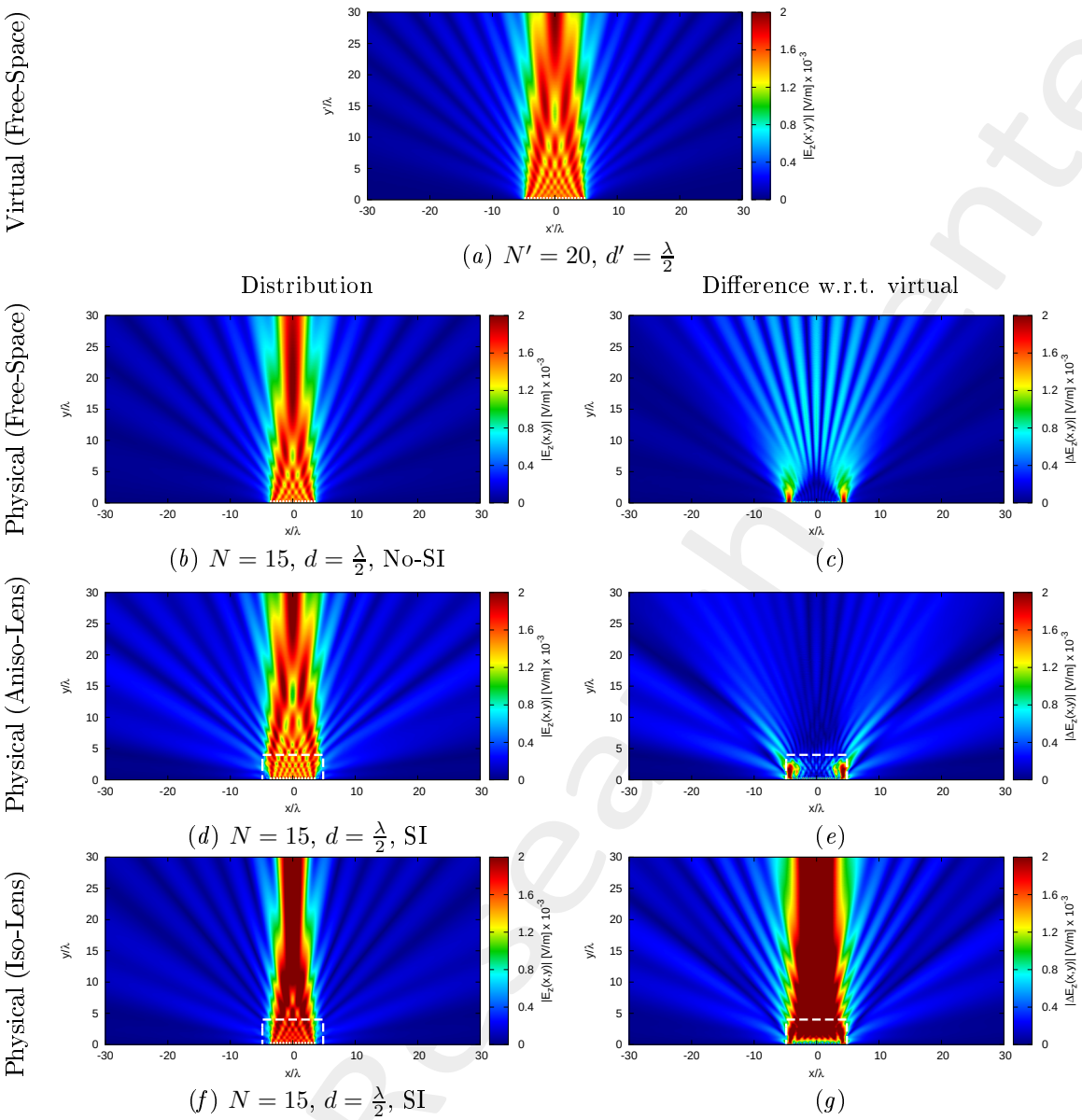

(a) $N' = 20$, $d' = \frac{\lambda}{2}$

(b) $N = 15$, $d = \frac{\lambda}{2}$, No-SI (c)

(d) $N = 15$, $d = \frac{\lambda}{2}$, SI (e)

(f) $N = 15$, $d = \frac{\lambda}{2}$, SI (g)

Figure 28: $\phi_s = 90$ [deg], $f = 600$ [MHz] - Electric field distributions.

1.3.3 Far-Field Patterns ($\phi_s = 90$ [deg], $f = 600$ [MHz])

Anisotropic Lens

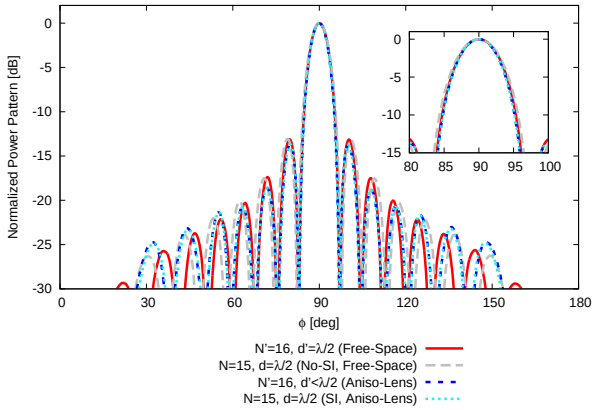

(a) $w' = 11.0$ $[\lambda]$, $N' = 16$

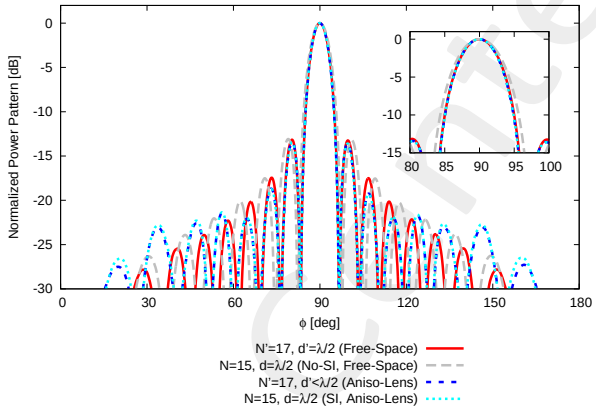

(b) $w' = 11.7$ $[\lambda]$, $N' = 17$

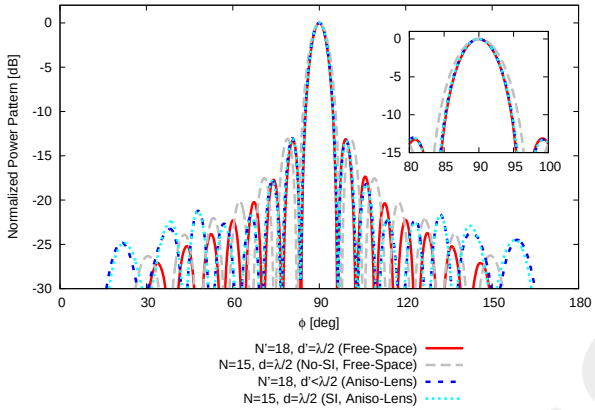

(c) $w' = 12.4$ $[\lambda]$, $N' = 18$

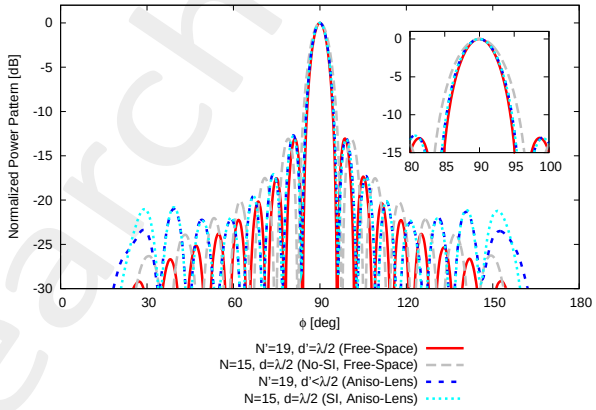

(d) $w' = 13.0$ $[\lambda]$, $N' = 19$

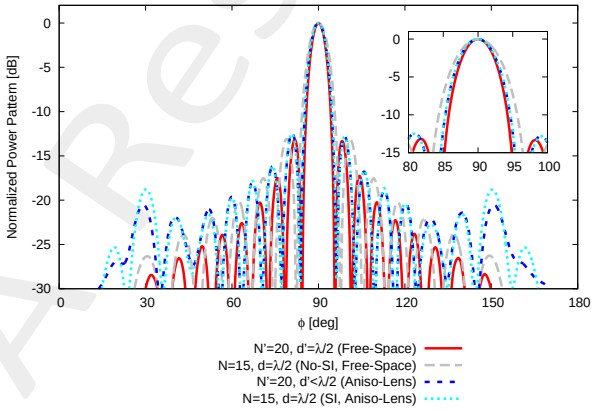

(e) $w' = 13.6$ $[\lambda]$, $N' = 20$

Figure 29: $\phi_s = 90$ [deg], $f = 600$ [MHz] - Far field pattern comparison for different values of w'.

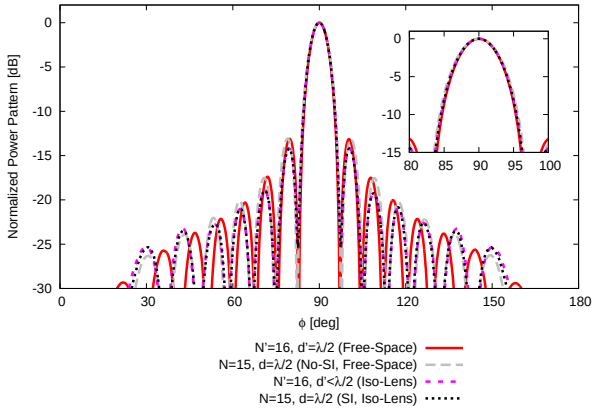

(a) $w' = 11.0$ $[\lambda]$, $N' = 16$

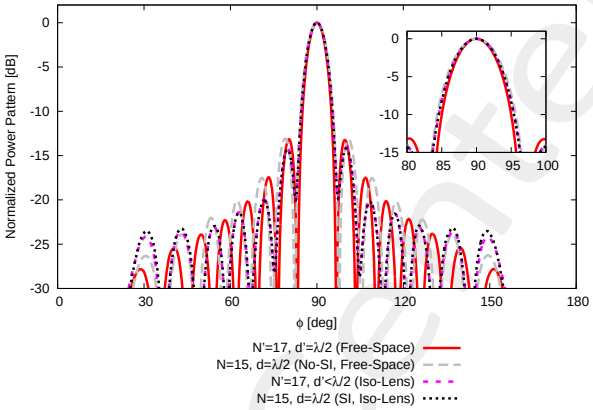

(b) $w' = 11.7$ $[\lambda]$, $N' = 17$

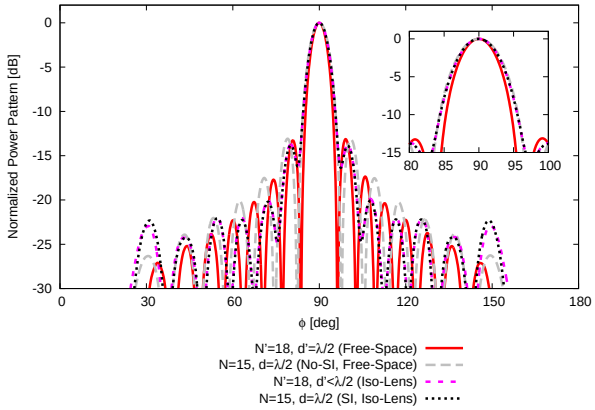

(c) $w' = 12.4$ $[\lambda]$, $N' = 18$

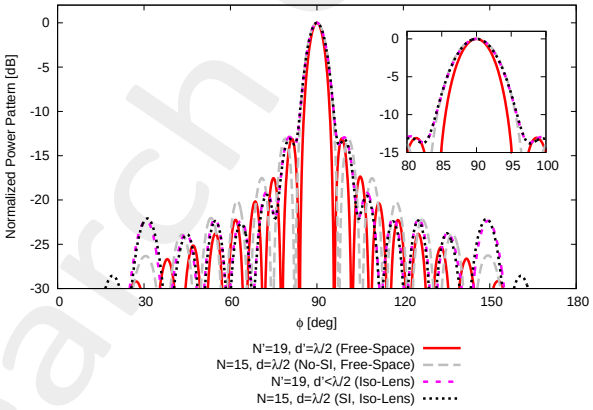

(d) $w' = 13.0$ $[\lambda]$, $N' = 19$

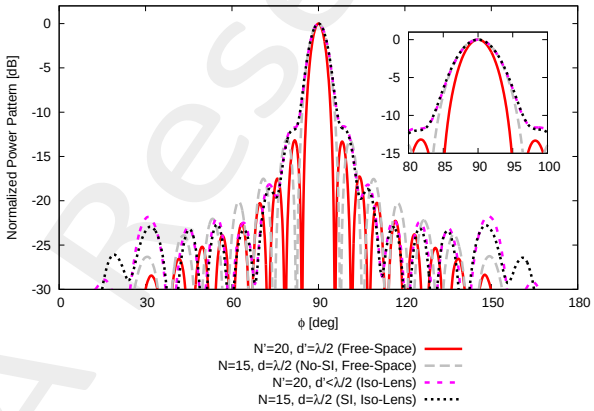

(e) $w' = 13.6$ $[\lambda]$, $N' = 20$

Figure 30: $\phi_s = 90$ [deg], $f = 600$ [MHz] - Far field pattern comparison for different values of w'.

1.3.4 Far-Field Patterns ($\phi_s = 75$ [deg], $f = 600$ [MHz])

Anisotropic Lens

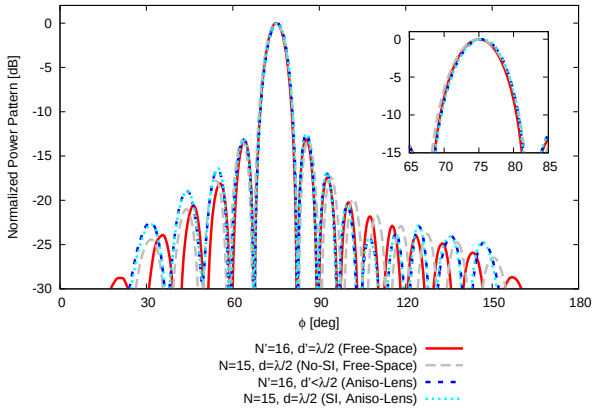

(a) $w' = 11.0$ $[\lambda]$, $N' = 16$

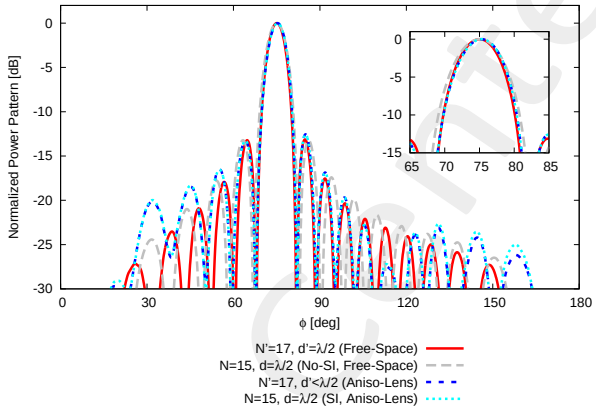

(b) $w' = 11.7$ $[\lambda]$, $N' = 17$

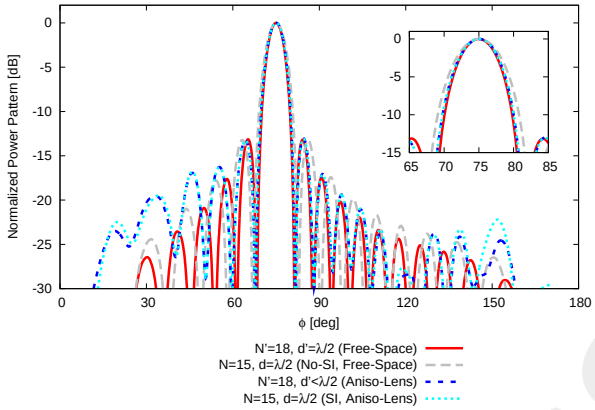

(c) $w' = 12.4$ $[\lambda]$, $N' = 18$

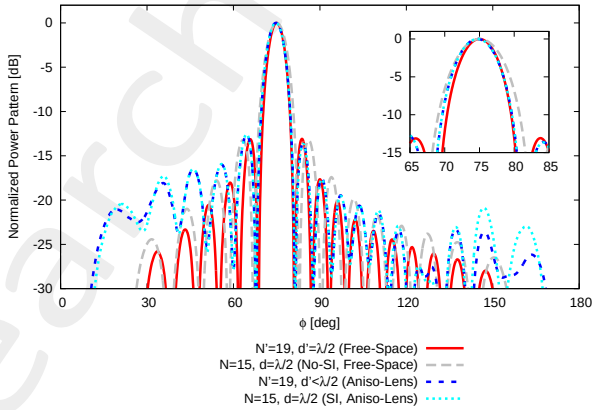

(d) $w' = 13.0$ $[\lambda]$, $N' = 19$

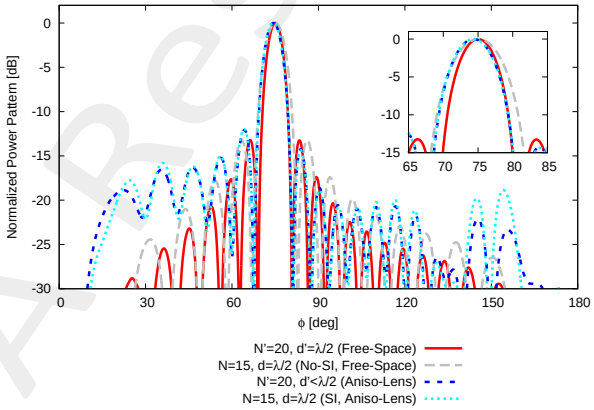

(e) $w' = 13.6$ $[\lambda]$, $N' = 20$

Figure 31: $\phi_s = 75$ [deg], $f = 600$ [MHz] - Far field pattern comparison for different values of w'.

1.3.5 Far-Field Patterns ($\phi_s = 60$ [deg], $f = 600$ [MHz])

Anisotropic Lens

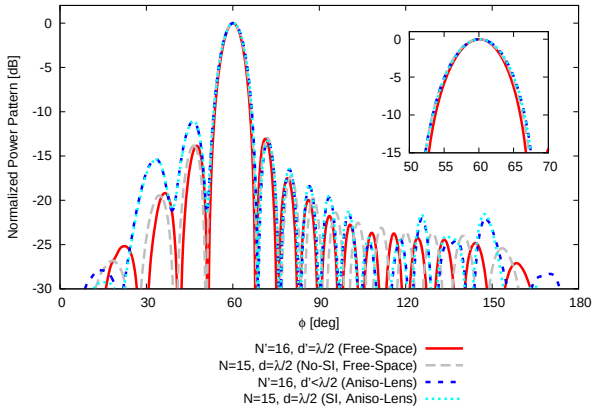

(a) $w' = 11.0$ $[\lambda]$, $N' = 16$

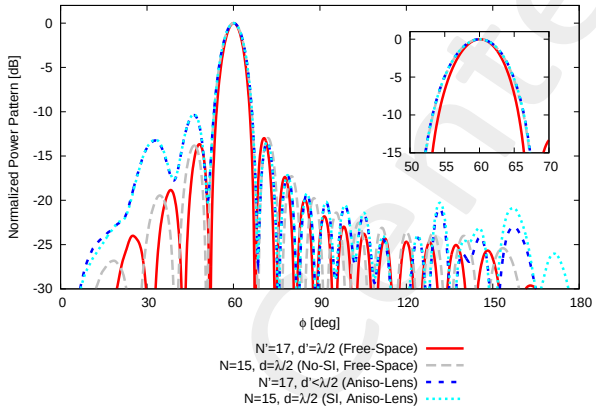

(b) $w' = 11.7$ $[\lambda]$, $N' = 17$

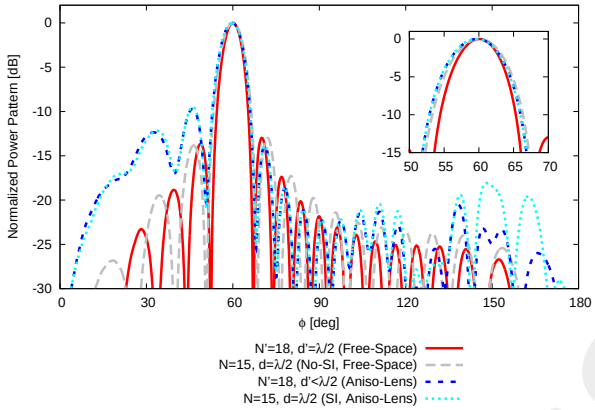

(c) $w' = 12.4$ $[\lambda]$, $N' = 18$

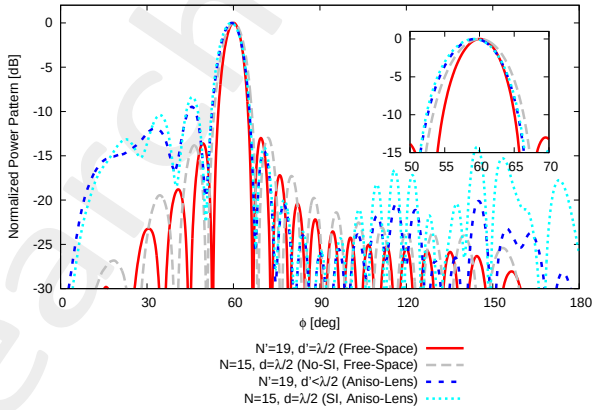

(d) $w' = 13.0$ $[\lambda]$, $N' = 19$

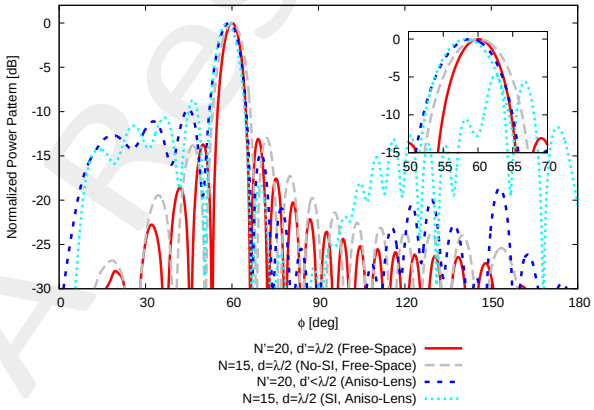

(e) $w' = 13.6$ $[\lambda]$, $N' = 20$

Figure 32: $\phi_s = 60$ [deg], $f = 600$ [MHz] - Far field pattern comparison for different values of w'.

1.3.6 Far-Field Patterns ($\phi_s = 105$ [deg], $f = 600$ [MHz])

Anisotropic Lens

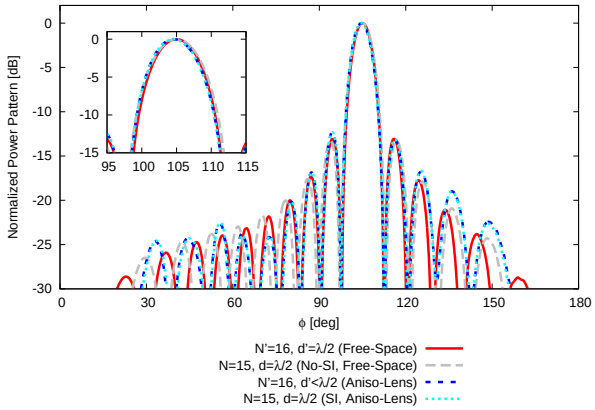

(a) $w' = 11.0$ $[\lambda]$, $N' = 16$

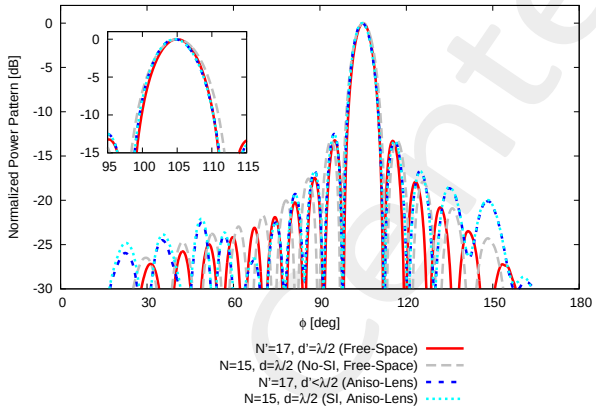

(b) $w' = 11.7$ $[\lambda]$, $N' = 17$

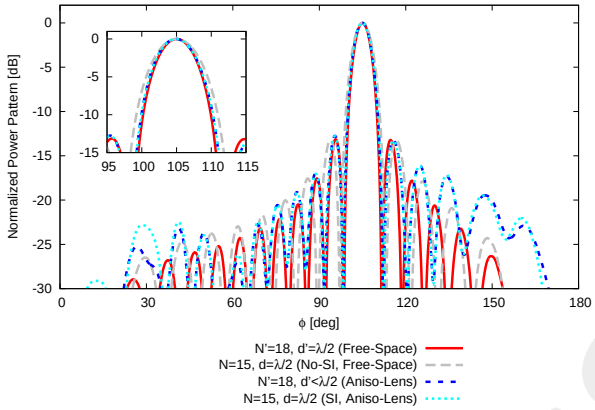

(c) $w' = 12.4$ $[\lambda]$, $N' = 18$

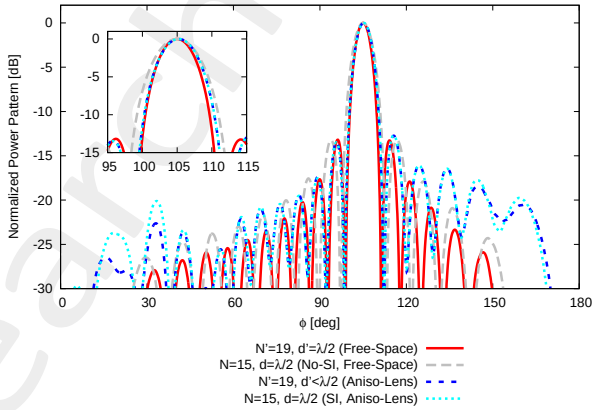

(d) $w' = 13.0$ $[\lambda]$, $N' = 19$

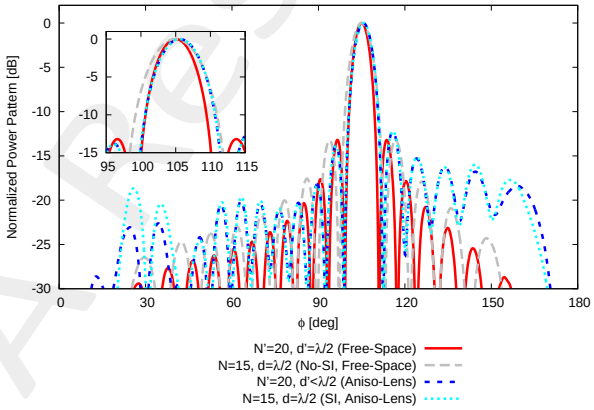

(e) $w' = 13.6$ $[\lambda]$, $N' = 20$

Figure 33: $\phi_s = 105$ [deg], $f = 600$ [MHz] - Far field pattern comparison for different values of w'.

1.3.7 Far-Field Patterns ($\phi_s = 120$ [deg], $f = 600$ [MHz])

Anisotropic Lens

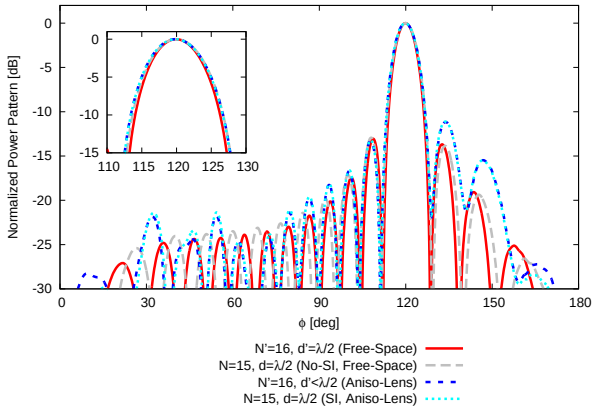

(a) $w' = 11.0$ $[\lambda]$, $N' = 16$

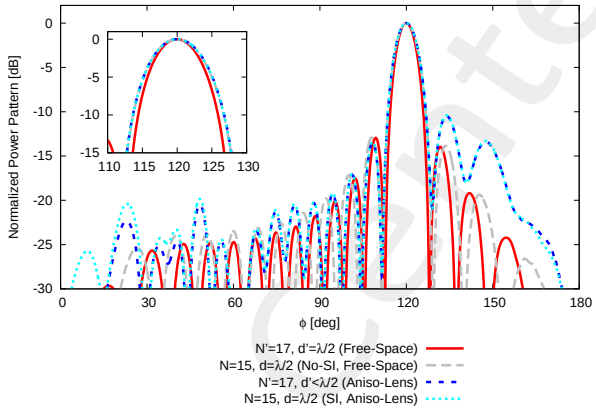

(b) $w' = 11.7$ $[\lambda]$, $N' = 17$

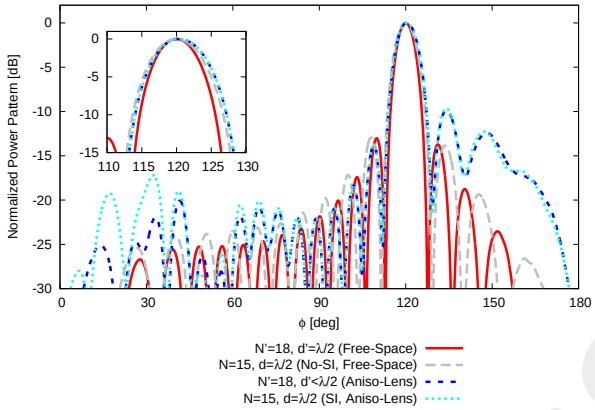

(c) $w' = 12.4$ $[\lambda]$, $N' = 18$

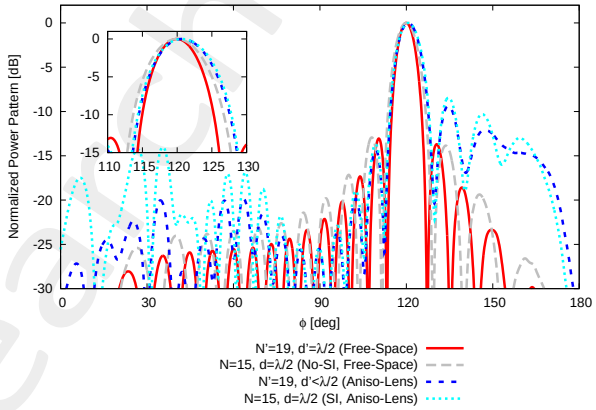

(d) $w' = 13.0$ $[\lambda]$, $N' = 19$

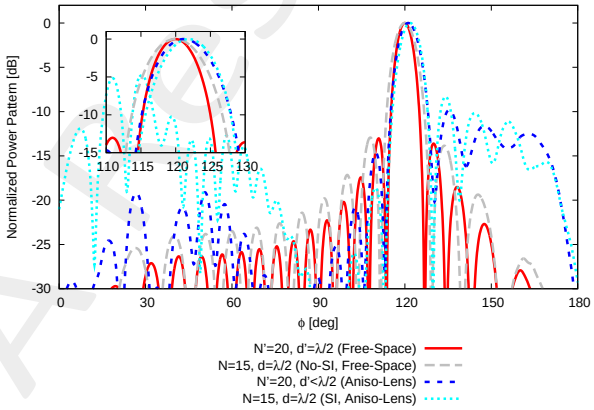

(e) $w' = 13.6$ $[\lambda]$, $N' = 20$

Figure 34: $\phi_s = 120$ [deg], $f = 600$ [MHz] - Far field pattern comparison for different values of w'.

1.3.8 Final Summary ($\phi_s = 90$ [deg], $f = 600$ [MHz])

$w' = 11.0$ [λ]				
	Virtual Array	**Physical Array**		
Environment	Free-Space	Free-Space (No-SI)	Aniso-Lens (SI)	Iso-Lens (SI)
Number of elements	16	15		
Spacing [λ]	0.5	0.5		
Aperture [λ]	7.5	7.0		
SLL [dB]	13.11	13.08	13.66	14.20
$FNBW$ [deg]	14.32	15.31	14.04	14.86
$3dB$ Beamwidth [deg]	6.36	6.76	6.15	6.44
Matching Error, ξ (w.r.t. virtual, outside lens)	-	3.24×10^{-1}	2.93×10^{-1}	5.85×10^{-1}

$w' = 11.7$ [λ]				
	Virtual Array	**Physical Array**		
Environment	Free-Space	Free-Space (No-SI)	Aniso-Lens (SI)	Iso-Lens (SI)
Number of elements	17	15		
Spacing [λ]	0.5	0.5		
Aperture [λ]	8.0	7.0		
SLL [dB]	13.16	13.08	13.46	14.19
$FNBW$ [deg]	13.60	15.31	13.42	14.68
$3dB$ Beamwidth [deg]	5.97	6.76	5.89	6.36
Matching Error, ξ (w.r.t. virtual, outside lens)	-	5.57×10^{-1}	4.09×10^{-1}	9.17×10^{-1}

$w' = 12.4$ [λ]				
	Virtual Array	**Physical Array**		
Environment	Free-Space	Free-Space (No-SI)	Aniso-Lens (SI)	Iso-Lens (SI)
Number of elements	18	15		
Spacing [λ]	0.5	0.5		
Aperture [λ]	8.5	7.0		
SLL [dB]	13.14	13.08	13.06	13.83
$FNBW$ [deg]	12.79	15.31	13.06	14.95
$3dB$ Beamwidth [deg]	5.64	6.76	5.75	6.44
Matching Error, ξ (w.r.t. virtual, outside lens)	-	6.60×10^{-1}	4.17×10^{-1}	1.14

$w' = 13.0$ [λ]				
	Virtual Array	**Physical Array**		
Environment	Free-Space	Free-Space (No-SI)	Aniso-Lens (SI)	Iso-Lens (SI)
Number of elements	19	15		
Spacing [λ]	0.5	0.5		
Aperture [λ]	9.0	7.0		
SLL [dB]	13.06	13.08	12.77	13.08
$FNBW$ [deg]	12.07	15.31	12.79	15.40
$3dB$ Beamwidth [deg]	5.35	6.76	5.65	6.59
Matching Error, ξ (w.r.t. virtual, outside lens)	-	6.46×10^{-1}	4.83×10^{-1}	1.39

$w' = 13.6$ [λ]				
	Virtual Array	**Physical Array**		
Environment	Free-Space	Free-Space (No-SI)	Aniso-Lens (SI)	Iso-Lens (SI)
Number of elements	20	15		
Spacing [λ]	0.5	0.5		
Aperture [λ]	9.5	7.0		
SLL [dB]	13.18	13.08	12.49	18.65
$FNBW$ [deg]	11.44	15.31	12.70	29.44
$3dB$ Beamwidth [deg]	5.06	6.76	5.62	6.86
Matching Error, ξ (w.r.t. virtual, outside lens)	-	6.37×10^{-1}	5.90×10^{-1}	1.56

Table V: $\phi_s = 90$ [deg], $f = 600$ [MHz] - Final summary.

1.3.9 Final Summary ($\phi_s = 75$ [deg], $f = 600$ [MHz])

$w' = 11.0$ [λ]				
	Virtual Array	**Physical Array**		
Environment	Free-Space	Free-Space (No-SI)	Aniso-Lens (SI)	Iso-Lens (SI)
Number of elements	16	15		
Spacing [λ]	0.5	0.5		
Aperture [λ]	7.5	7.0		
SLL [dB]	13.13	13.22	12.48	
$FNBW$ [deg]	14.86	15.94	15.04	
3dB Beamwidth [deg]	6.57	6.99	6.64	
Matching Error, ξ (w.r.t. virtual, outside lens)	-			

$w' = 11.7$ [λ]				
	Virtual Array	**Physical Array**		
Environment	Free-Space	Free-Space (No-SI)	Aniso-Lens (SI)	Iso-Lens (SI)
Number of elements	17	15		
Spacing [λ]	0.5	0.5		
Aperture [λ]	8.0	7.0		
SLL [dB]	13.13	13.22	12.57	
$FNBW$ [deg]	13.96	15.94	14.32	
3dB Beamwidth [deg]	6.17	6.99	6.29	
Matching Error, ξ (w.r.t. virtual, outside lens)	-			

$w' = 12.4$ [λ]				
	Virtual Array	**Physical Array**		
Environment	Free-Space	Free-Space (No-SI)	Aniso-Lens (SI)	Iso-Lens (SI)
Number of elements	18	15		
Spacing [λ]	0.5	0.5		
Aperture [λ]	8.5	7.0		
SLL [dB]	13.14	13.22	13.06	
$FNBW$ [deg]	13.24	15.94	13.87	
3dB Beamwidth [deg]	5.84	6.99	6.10	
Matching Error, ξ (w.r.t. virtual, outside lens)	-			

$w' = 13.0$ [λ]				
	Virtual Array	**Physical Array**		
Environment	Free-Space	Free-Space (No-SI)	Aniso-Lens (SI)	Iso-Lens (SI)
Number of elements	19	15		
Spacing [λ]	0.5	0.5		
Aperture [λ]	9.0	7.0		
SLL [dB]	13.09	13.22	12.57	
$FNBW$ [deg]	12.43	15.94	13.60	
3dB Beamwidth [deg]	5.54	6.99	5.99	
Matching Error, ξ (w.r.t. virtual, outside lens)	-			

$w' = 13.6$ [λ]				
	Virtual Array	**Physical Array**		
Environment	Free-Space	Free-Space (No-SI)	Aniso-Lens (SI)	Iso-Lens (SI)
Number of elements	20	15		
Spacing [λ]	0.5	0.5		
Aperture [λ]	9.5	7.0		
SLL [dB]	13.22	13.22	11.98	
$FNBW$ [deg]	11.89	15.94	13.60	
3dB Beamwidth [deg]	5.25	6.99	6.01	
Matching Error, ξ (w.r.t. virtual, outside lens)	-			

Table VI: $\phi_s = 75$ [deg], $f = 600$ [MHz] - Final summary.

1.3.10 Final Summary ($\phi_s = 60$ [deg], $f = 600$ [MHz])

$w' = 11.0$ [λ]				
	Virtual Array	**Physical Array**		
Environment	Free-Space	Free-Space (No-SI)	Aniso-Lens (SI)	Iso-Lens (SI)
Number of elements	16	15		
Spacing [λ]	0.5	0.5		
Aperture [λ]	7.5	7.0		
SLL [dB]	13.06	12.98	11.05	
$FNBW$ [deg]	16.66	17.74	17.65	
3dB Beamwidth [deg]	7.31	7.81	7.88	
Matching Error, ξ (w.r.t. virtual, outside lens)	-			

$w' = 11.7$ [λ]				
	Virtual Array	**Physical Array**		
Environment	Free-Space	Free-Space (No-SI)	Aniso-Lens (SI)	Iso-Lens (SI)
Number of elements	17	15		
Spacing [λ]	0.5	0.5		
Aperture [λ]	8.0	7.0		
SLL [dB]	12.99	12.98	10.29	
$FNBW$ [deg]	15.67	17.74	17.47	
3dB Beamwidth [deg]	6.90	7.81	7.90	
Matching Error, ξ (w.r.t. virtual, outside lens)	-			

$w' = 12.4$ [λ]				
	Virtual Array	**Physical Array**		
Environment	Free-Space	Free-Space (No-SI)	Aniso-Lens (SI)	Iso-Lens (SI)
Number of elements	18	15		
Spacing [λ]	0.5	0.5		
Aperture [λ]	8.5	7.0		
SLL [dB]	12.98	12.98	9.48	
$FNBW$ [deg]	14.77	17.74	17.29	
3dB Beamwidth [deg]	6.51	7.81	7.93	
Matching Error, ξ (w.r.t. virtual, outside lens)	-			

$w' = 13.0$ [λ]				
	Virtual Array	**Physical Array**		
Environment	Free-Space	Free-Space (No-SI)	Aniso-Lens (SI)	Iso-Lens (SI)
Number of elements	19	15		
Spacing [λ]	0.5	0.5		
Aperture [λ]	9.0	7.0		
SLL [dB]	13.00	12.98	8.36	
$FNBW$ [deg]	13.96	17.74	17.29	
3dB Beamwidth [deg]	6.16	7.81	8.15	
Matching Error, ξ (w.r.t. virtual, outside lens)	-			

$w' = 13.6$ [λ]				
	Virtual Array	**Physical Array**		
Environment	Free-Space	Free-Space (No-SI)	Aniso-Lens (SI)	Iso-Lens (SI)
Number of elements	20	15		
Spacing [λ]	0.5	0.5		
Aperture [λ]	9.5	7.0		
SLL [dB]	13.10	12.98	5.84	
$FNBW$ [deg]	13.33	17.74	16.39	
3dB Beamwidth [deg]	5.85	7.81	7.22	
Matching Error, ξ (w.r.t. virtual, outside lens)	-			

Table VII: $\phi_s = 60$ [deg], $f = 600$ [MHz] - Final summary.

1.3.11 Final Summary ($\phi_s = 105$ [deg], $f = 600$ [MHz])

$w' = 11.0$ [λ]				
	Virtual Array	**Physical Array**		
Environment	Free-Space	Free-Space (No-SI)	Aniso-Lens (SI)	Iso-Lens (SI)
Number of elements	16	15		
Spacing [λ]	0.5	0.5		
Aperture [λ]	7.5	7.0		
SLL [dB]	13.06	13.24	12.32	
$FNBW$ [deg]	14.86	15.94	15.04	
3dB Beamwidth [deg]	6.57	7.01	6.65	
Matching Error, ξ (w.r.t. virtual, outside lens)	-			

$w' = 11.7$ [λ]				
	Virtual Array	**Physical Array**		
Environment	Free-Space	Free-Space (No-SI)	Aniso-Lens (SI)	Iso-Lens (SI)
Number of elements	17	15		
Spacing [λ]	0.5	0.5		
Aperture [λ]	8.0	7.0		
SLL [dB]	13.23	13.24	12.53	
$FNBW$ [deg]	14.05	15.94	14.41	
3dB Beamwidth [deg]	6.17	7.01	6.34	
Matching Error, ξ (w.r.t. virtual, outside lens)	-			

$w' = 12.4$ [λ]				
	Virtual Array	**Physical Array**		
Environment	Free-Space	Free-Space (No-SI)	Aniso-Lens (SI)	Iso-Lens (SI)
Number of elements	18	15		
Spacing [λ]	0.5	0.5		
Aperture [λ]	8.5	7.0		
SLL [dB]	13.14	13.24	12.80	
$FNBW$ [deg]	13.24	15.94	13.96	
3dB Beamwidth [deg]	5.84	7.01	6.13	
Matching Error, ξ (w.r.t. virtual, outside lens)	-			

$w' = 13.0$ [λ]				
	Virtual Array	**Physical Array**		
Environment	Free-Space	Free-Space (No-SI)	Aniso-Lens (SI)	Iso-Lens (SI)
Number of elements	19	15		
Spacing [λ]	0.5	0.5		
Aperture [λ]	9.0	7.0		
SLL [dB]	13.19	13.24	12.69	
$FNBW$ [deg]	12.61	15.94	13.78	
3dB Beamwidth [deg]	5.54	7.01	6.03	
Matching Error, ξ (w.r.t. virtual, outside lens)	-			

$w' = 13.6$ [λ]				
	Virtual Array	**Physical Array**		
Environment	Free-Space	Free-Space (No-SI)	Aniso-Lens (SI)	Iso-Lens (SI)
Number of elements	20	15		
Spacing [λ]	0.5	0.5		
Aperture [λ]	9.5	7.0		
SLL [dB]	13.20	13.24	12.21	
$FNBW$ [deg]	11.89	15.94	13.69	
3dB Beamwidth [deg]	5.26	7.01	6.03	
Matching Error, ξ (w.r.t. virtual, outside lens)	-			

Table VIII: $\phi_s = 105$ [deg], $f = 600$ [MHz] - Final summary.

1.3.12 Final Summary ($\phi_s = 120$ [deg], $f = 600$ [MHz])

$w' = 11.0$ [λ]				
	Virtual Array	**Physical Array**		
Environment	Free-Space	Free-Space (No-SI)	Aniso-Lens (SI)	Iso-Lens (SI)
Number of elements	16	15		
Spacing [λ]	0.5	0.5		
Aperture [λ]	7.5	7.0		
SLL [dB]	13.05	12.93	11.12	
$FNBW$ [deg]	16.66	17.74	17.65	
3dB Beamwidth [deg]	7.30	7.77	7.90	
Matching Error, ξ (w.r.t. virtual, outside lens)	-			

$w' = 11.7$ [λ]				
	Virtual Array	**Physical Array**		
Environment	Free-Space	Free-Space (No-SI)	Aniso-Lens (SI)	Iso-Lens (SI)
Number of elements	17	15		
Spacing [λ]	0.5	0.5		
Aperture [λ]	8.0	7.0		
SLL [dB]	12.95	12.93	10.42	
$FNBW$ [deg]	15.67	17.74	17.38	
3dB Beamwidth [deg]	6.86	7.77	7.88	
Matching Error, ξ (w.r.t. virtual, outside lens)	-			

$w' = 12.4$ [λ]				
	Virtual Array	**Physical Array**		
Environment	Free-Space	Free-Space (No-SI)	Aniso-Lens (SI)	Iso-Lens (SI)
Number of elements	18	15		
Spacing [λ]	0.5	0.5		
Aperture [λ]	8.5	7.0		
SLL [dB]	13.02	12.93	9.65	
$FNBW$ [deg]	14.77	17.74	17.29	
3dB Beamwidth [deg]	6.50	7.77	8.00	
Matching Error, ξ (w.r.t. virtual, outside lens)	-			

$w' = 13.0$ [λ]				
	Virtual Array	**Physical Array**		
Environment	Free-Space	Free-Space (No-SI)	Aniso-Lens (SI)	Iso-Lens (SI)
Number of elements	19	15		
Spacing [λ]	0.5	0.5		
Aperture [λ]	9.0	7.0		
SLL [dB]	13.06	12.93	8.44	
$FNBW$ [deg]	13.96	17.74	17.47	
3dB Beamwidth [deg]	6.15	7.77	8.26	
Matching Error, ξ (w.r.t. virtual, outside lens)	-			

$w' = 13.6$ [λ]				
	Virtual Array	**Physical Array**		
Environment	Free-Space	Free-Space (No-SI)	Aniso-Lens (SI)	Iso-Lens (SI)
Number of elements	20	15		
Spacing [λ]	0.5	0.5		
Aperture [λ]	9.5	7.0		
SLL [dB]	13.03	12.93	5.91	
$FNBW$ [deg]	13.24	17.74	16.84	
3dB Beamwidth [deg]	5.85	7.77	7.29	
Matching Error, ξ (w.r.t. virtual, outside lens)	-			

Table IX: $\phi_s = 120$ [deg], $f = 600$ [MHz] - Final summary.

1.3.13 Final Summary: Performances vs. w' (vs. N')

Anisotropic Lens

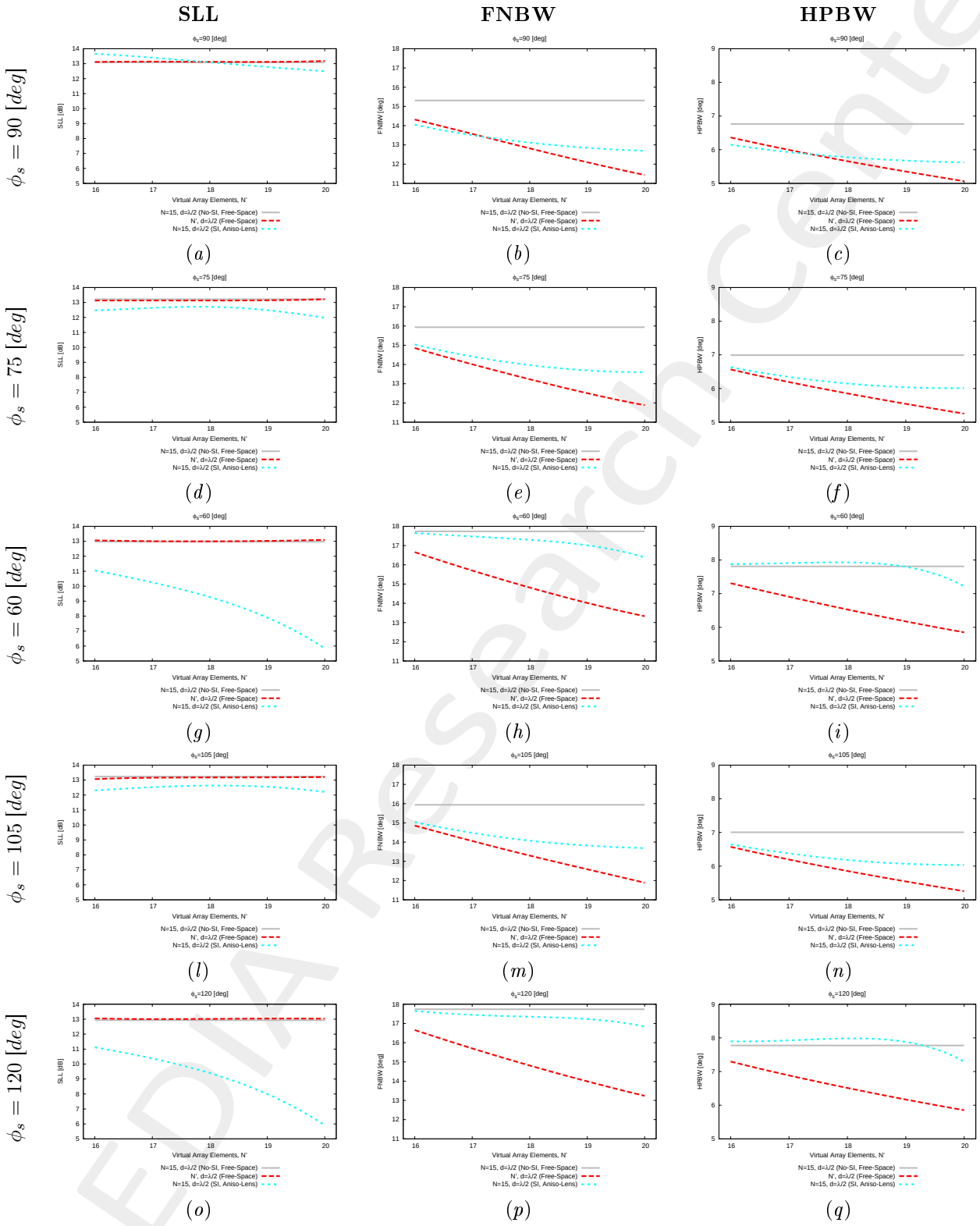

Figure 35: Aniso-Lens, $f = 600$ [MHz] - Pattern performances vs w' (vs. N').

1.3.14 Final Summary: Performances vs. Steering Angle (ϕ_s)

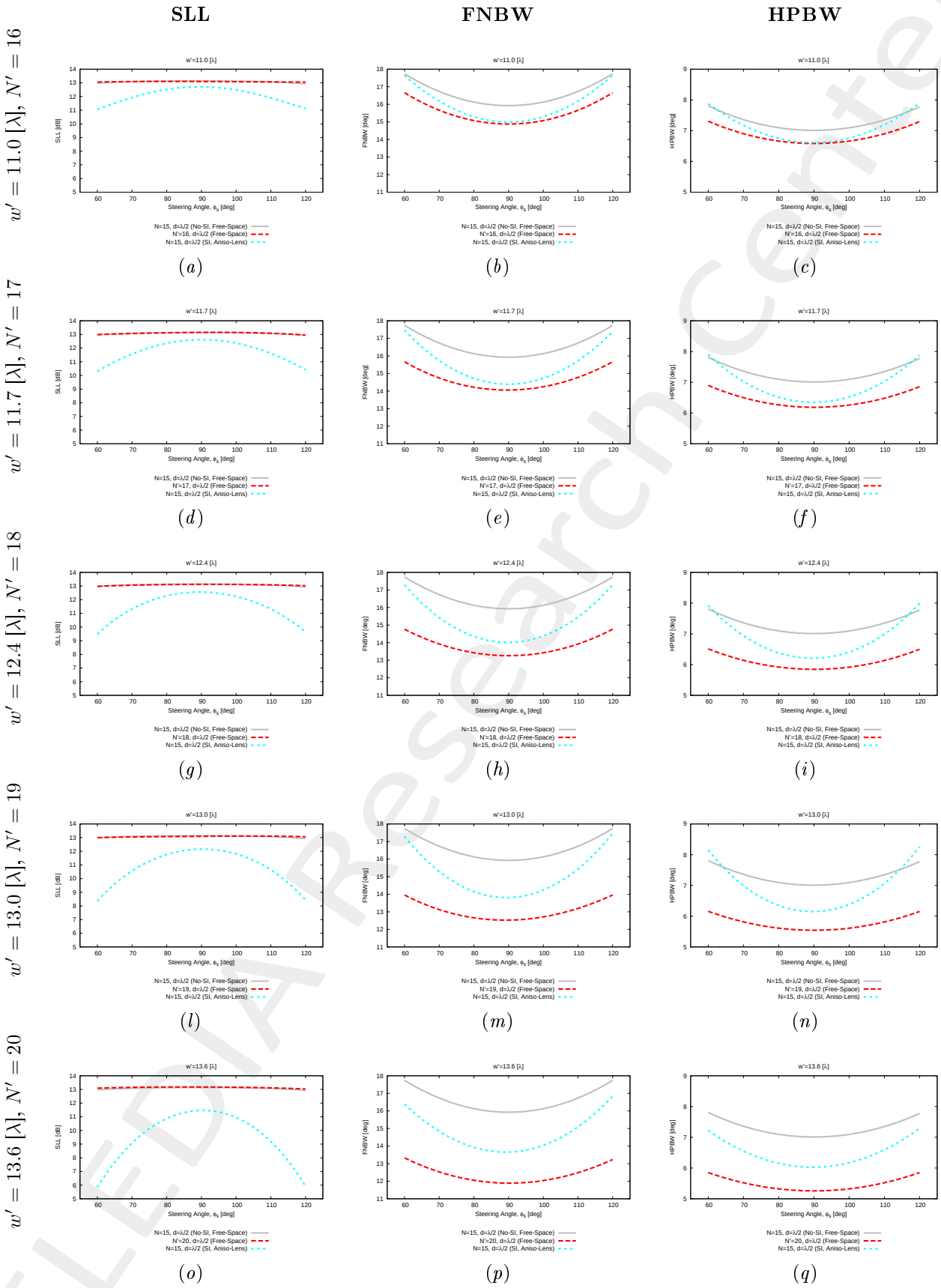

Figure 36: Aniso-Lens, $f = 600$ [MHz] - Pattern performances vs w' (vs. N').

References

[1] G. Oliveri, G. Gottardi, F. Robol, A. Polo, L. Poli, M. Salucci, M. Chuan, C. Massagrande, P. Vinetti, M. Mattivi, R. Lombardi, and A. Massa, "Co-design of unconventional array architectures and antenna elements for 5G base station," *IEEE Trans. Antennas Propag.*, vol. 65, no. 12, pp. 6752-6767, Dec. 2017.

[2] P. Rocca, G. Oliveri, R. J. Mailloux, and A. Massa, "Unconventional phased array architectures and design methodologies - A review," *Proc. IEEE*, vol. 104, no. 3, pp. 544-560, Mar. 2016.

[3] G. Oliveri, M. Salucci, N. Anselmi and A. Massa, "Multiscale System-by-Design synthesis of printed WAIMs for waveguide array enhancement," *IEEE J. Multiscale Multiphysics Computat. Techn.*, vol. 2, pp. 84-96, 2017.

[4] A. Massa and G. Oliveri, "Metamaterial-by-Design: Theory, methods, and applications to communications and sensing - Editorial," *EPJ Applied Metamaterials*, vol. 3, no. E1, pp. 1-3, 2016.

[5] L. Poli, G. Oliveri, P. Rocca, M. Salucci, and A. Massa, "Long-Distance WPT Unconventional Arrays Synthesis," *J. Electromagnet. Wave.*, vol. 31, no. 14, pp. 1399-1420, Jul. 2017.

[6] G. Oliveri, F. Viani, N. Anselmi, and A. Massa, "Synthesis of multi-layer WAIM coatings for planar phased arrays within the system-by-design framework," *IEEE Trans. Antennas Propag.*, vol. 63, no. 6, pp. 2482-2496, Jun. 2015.

[7] G. Oliveri, L. Tenuti, E. Bekele, M. Carlin, and A. Massa, "An SbD-QCTO approach to the synthesis of isotropic metamaterial lenses," *IEEE Antennas Wireless Propag. Lett.*, vol. 13, pp. 1783-1786, 2014.

[8] G. Oliveri, D. H. Werner, and A. Massa, "Reconfigurable electromagnetics through metamaterials - A review" *Proc. IEEE*, vol. 103, no. 7, pp. 1034-1056, Jul. 2015.

[9] G. Oliveri, E. T. Bekele, M. Salucci, and A. Massa, "Transformation electromagnetics miniaturization of sectoral and conical horn antennas," *IEEE Trans. Antennas Propag.*, vol. 64, no. 4, pp. 1508-1513, Apr. 2016.

[10] G. Oliveri, E. T. Bekele, M. Salucci, and A. Massa, "Array miniaturization through QCTO-SI metamaterial radomes," *IEEE Trans. Antennas Propag.*, vol. 63, no. 8, pp. 3465-3476, Aug. 2015.

[11] G. Oliveri, E. T. Bekele, D. H. Werner, J. P. Turpin, and A. Massa, "Generalized QCTO for metamaterial-lens-coated conformal arrays," *IEEE Trans. Antennas Propag.*, vol. 62, no. 8, pp 4089-4095, Aug. 2014.

[12] G. Oliveri, E. Bekele, M. Carlin, L. Tenuti, J. Turpin, D. H. Werner, and A. Massa, "Extended QCTO for innovative antenna system designs," IEEE Antenna Conference on Antenna Measurements and Applications (CAMA 2014), pp. 1-3, Nov. 16-19, 2014.

[13] G. Oliveri, P. Rocca, M. Salucci, E. T. Bekele, D. H. Werner, and A. Massa, "Design and synthesis of innovative metamaterial-enhanced arrays," IEEE International Symposium on Antennas Propag. (APS/URSI 2013), Orlando, Florida, USA, pp. 972 - 973, Jul. 7-12, 2013.

[14] G. Oliveri, "Improving the reliability of frequency domain simulators in the presence of homogeneous metamaterials - A preliminary numerical assessment," *Progress In Electromagnetics Research*, vol. 122, pp. 497-518, 2012.

[15] M. Salucci, G. Oliveri, N. Anselmi, G. Gottardi, and A. Massa, "Performance enhancement of linear active electronically-scanned arrays by means of MbD-synthesized metalenses," *J. Electromagnet. Wave.*, vol. 0, no. 0, pp. 1-29, 2017 (DOI: 10.1080/09205071.2017.1410077).